Supporting Information

Dual-modal Imaging-Guided Agent Based on NIR-II Aggregation-Induced Emission Luminogens with Balanced Phototheranostic Performance

Chengjun Dong,[a]+ Ziwen Zhang,[b]+ Hongyu Wu,[b] Xinting Liang,[a] Shihao Pang,[a] Kehuan Wu,[b] Jie Sun,[a] Xuemei Dong,[a] Lixin Sun,[a]Xianfeng Gu,[b] Chunchang Zhao*[a]*

[a]Key Laboratory for Advanced Materials and Feringa Nobel Prize Scientist Joint Research Center, Institute of Fine Chemicals, School of Chemistry and Molecular Engineering, Frontiers Science Center for Materiobiology and Dynamic Chemistry, East China University of Science and Technology, Shanghai, 200237, P. R. China.

[b]Department of Medicinal Chemistry, School of Pharmacy, Fudan University, Shanghai, 201203, P. R. China.

**Corresponding authors:* xfgu@fudan.edu.cn (X. Gu), zhaocchang@ecust.edu.cn (C. Zhao)

[+]*C.D. and Z.Z. contributed equally to this work*

Table of Contents

1.Experimental section

Main materials

Commercially available chemicals, such as 2-Formyl-5-bromothiophene, 9,10-diazaanthracene, n-BuLi, $Pd_2(dba)_3$, $Pd(PPh_3)_4$, t-BuONa *et al*. were obtained from Adamas, TCI, Sigma-Aldrich and Bide and used as received unless otherwise stated. All solvents were purified and dried before use by standard methods. The solvents used in spectrum analysis were HPLC-grade.

MCF-7, RAW 264.7 and Hela cells were purchased from Cell Bank of the Chi nese Academy of Sciences. 1,2-Distearoyl-sn-glycero-3-phosphoethanolamine-N[m ethoxy(polyethylene glycol)-2000] (DSPE-PEG2000) were purchased from Laysa n Bio, Inc.(USA) and 1,2-Distearoylsn-glycero-3-phosphoethanolamine-N-(polyeth ylene glycol)-folic acid (DSPE-PEG2000-FA) were purchased from Chongqing Yu Si Medical Technology Co., LTD (China). Living/Dead cell double staining kitCalcein-AM were purchased from Beyotime Biotech Inc. (China).

Instruments

^1H and ^{13}C NMR spectra were recorded with a Bruker ARX 400/600 NMR spectrometer using C_6D_6, C_3D_6O as solvent. Mass spectra were obtained on a HP 1100 LCMS spectrometer. UV-vis absorption spectra were acquired on a Varian Cary 100 spectrophotometer. Photothermal experiments were implemented by using an 808 nm infrared semiconductor laser (Changchun radium photoelectric technology). Temperature changes were recorded by an E6 IR thermal camera (FLIR Systems). CCK-8 assays were conducted on a Bio Tek microplate reader.

Theoretical simulation

All theoretical simulations are performed on the Gaussian 16 A03 package.[1] For density-functional theory (DFT) calculations, ground-state (S_0) molecular geometries are optimized at B3LYP/6-31G (d, p) level. For time-dependent DFT (TD-DFT) simulations, molecular geometry optimization in the first singlet excited state (S_1) is

calculated in B3LYP/6-31G (d, p) level. The electrostatic potential is then calculated based on the optimized S_1 molecular geometries at the same level and analyzed with Multiwfn 3.8 code.[2]

Preparation of FA-SC and FA-LSC NPs.

100 μL of DMSO solution containing 2 mg of compound **SC** or **LSC**, 8 mg of DSPE-mPEG2000, and 4 mg DSPE-mPEG2000-FA was poured into 2 mL of deionized water. Followed by sonication with a microtip probe sonicator at 45% output power for 15 min continuously. Then the mixtures were transferred into dialysis tube (MWCO 1000 Da) and dialyzed against deionized water for 8 h. To remove DMSO completely, the water was replaced by fresh water every 2 h. Finally, the samples were filtered using a 0.22 μm pore size membrane and store at 4 ℃ in dark. As control materials, PEG-SC and PEG-LSC NPs were prepared as the above-mentioned method using DSPE-mPEG2000 instead of DSPE-mPEG2000-FA, while FA-ICG NPs and PEG-ICG NPs were prepared using ICG instead of **SC**.

Photothermal performance measurement

The PBS solution of **FA-DC**, **FA-SC**, **FA-LSC NPs** with the specified concentrations were continuously exposed to 808 nm laser at appointed power density. The temperature was measured every 30 s and stopped until the temperature nearly reached to a plateau. In addition, different concentrations of NPs (50, 100, 200, 400 μg mL^{-1} were placed under 808 nm laser (2 W cm^{-2}) for 10 min, and the increasing temperature was detected via FLIR. The corresponding infrared thermal images of the sample tubes were also acquired. And similar operations were conducted to evaluate the photothermal performance of their nanoparticle forms in aqueous solutions. Pure PBS solution under the same condition served as the control groups, respectively. In addition, the photothermal conversion efficiency (η) of **FA-DC**, **FA-SC**, **FA-LSC NPs** in aqueous solution was calculated according to the literature. [4]

Photostability tests

Two milliliter of **FA-LSC NPs** (200 μg mL^{-1}) was placed under 808 nm laser (2 W cm^{-}

^{2}) for continuous irradiation for 10 min, then turned off the laser and waited for it to cool down. Repeated the heating and cooling cycle process was repeated for four times, and the temperature of the solution was recorded by FLIR.

Fluorescence quantum yield measurement

A stock solution of IR-26 (the reference (QY = 0.5%)) in 1,2-dichloroethane was diluted to obtain a series of samples with absorbance values of ~ 0.05, ~0.03, ~0.02, ~0.01, and ~0.005 at 808 nm measured by UV-Vis-spectroscopy, respectively. And then, the 808 nm laser was used as the exciting light to acquire NIR-II emission spectra of the five solutions in the wavelength region of 900-1450 nm. The integrated fluorescence intensity was plotted against absorbance values at 808 nm and fitted into linear function. The same absorption and emission measurements were performed for **FA-DC NPs**, **FA-SC NPs** and **FA-LSC NPs** in aqueous solutions. According to the calculated slopes of the linear fitting curve, the quantum yields of the samples are calculated with IR-26 as the reference according to the following formula

$$QY_{\text{sample}} = QY_{\text{ref}} \cdot \frac{slope_{\text{sample}}}{slope_{\text{ref}}} \cdot \left(\frac{n_{sample}}{n_{\text{ref}}}\right)^2$$

where QY_{ref} is = 0.5 %, n_{sample} and n_{ref} are the refractive index of pure water and 1,2dichloroethane.

Cell culture

Hela cells, MCF-7 cells and RAW 264.7 cells were cultured at 37 °C in a humidified atmosphere of 5/95 CO_2/air incubator within Dulbecco's Eagle Medium (DMEM) supplemented with 10% fetal bovine serum (FBS). These cells were seeded in glass bottom dishes and allowed to adhere for 24 h prior to experiments.

Cytotoxicity evaluation

Hela and RAW 264.7 cells were seeded in a 96-well plate with a density of 5×10^5 cells per well. After 24 h incubation, different concentrations of **FA-LSC NPs** were added in the wells and incubated with cells for another 24 h. CCK-8 assay was used to stain the cells and the cytotoxicity was measured by microplate reader (excitation: 570 nm).

Flow cytometer assay

Hela cells were incubated into a 6-well plate and treated with different treatments (control, NPs, 808 nm laser irradiation, NPs + 808 nm laser irradiation). After 12 h, cells were collected and stained with propidium iodide (PI) and Annexin V-FITC. Finally, 10^5 treated cells were detected by a flow cytometer.

Cellular uptake

Hela cells and MCF-7 cells were cultured at a density of 2×10^5 per well in Petri dishes (35 mm Glass Bottom Confocal Dishes, Beyotime). ICG was used instead of **SC**/**LSC** to verify the in vitro active targeting of the developed probes. In brief, FA-ICG NPs and PEG-ICG NPs (C_{ICG} = 200 μg mL^{-1}) were incubated with Hela cells for 30, 60, 120, 180, 360 min. FA-ICG NPs were incubated with MCF-7 cells for 30, 60, 120, 180, 360 min. Free FA (3mg mL^{-1}) was used to treat Hela cells with high expression of folate receptor. Finally, the samples were observed using a confocal laser scanning microscope.

Live-dead cell staining

The Hela cells were seeded cultured in glass bottom dish for 24 h, **FA-LSC NPs** (200 μg mL^{-1}) were then added into the cell culture medium. After 6 h incubation, the cells were washed and replaced with fresh medium, followed by 808 nm laser irradiation (2 W cm^{-2}) for 8 min. After that, the cells were incubated at 37 °C for another 12 h, then successively stained with PI (60 μg mL^{-1}) and AM (2 μL mL^{-1}) in PBS for 10 min. Subsequently, the cells were gently washed and then imaged by CLSM. Conditions: excitation wavelength: 488 nm for AM and 534 nm for PI; emission filter: 490 - 540 nm for AM and 590 - 650 nm for PI.

Animal mode

Animal experiments were performed in rigid accordance with the relevant laws and institutional guidelines developed by the Fudan University's Administrative panel on Laboratory Animal Care, and the experiments were approved by the committee. Subcutaneous injection of Hela cells (6.0×10^6) suspended in 200 μL to the indicated location in female nude mice (4 - 5 weeks) was performed to establish the xenograft

Hela tumor-bearing mouse model. The mice with tumor size at about 40 - 50 mm^3 were used subsequently for PTT experiments.

In vivo NIR-II fluorescence and photothermal imaging

The Hela tumor-bearing mice were administered with **FA-LSC NPs** in saline at a dose of 200 μg **FA-LSC NPs** per mouse via tail vein. Then, at 0, 6, 12, and 24 h post-injection, the mice were anesthetized using 2% isoflurane in oxygen and imaged through a commercial measurement purchased from Suzhou NIR-Optics Technologies CO., Ltd., with the long pass (LP) filter of 1100 nm. For in vivo photothermal imaging, the infrared thermal images of mice were acquired using a 640 × 512pixel 2D InGaAs NIRvana CCD camera during the irradiation of 808 nm laser (2 W cm^{-2}) for 10 min at 12 h after administration with **FA-LSC NPs**. Mouse injected with saline under the same irradiation condition was used as the control. Images were processed with the LightField imaging software, ImageJ.

In vivo phototherapeutic study

When the inoculated tumor grew for 8 days, Hela tumor-bearing female nude mice were randomly divided into five groups (5 mice per group), named "PBS", "AIE NPs", "PBS + L" and "AIE NPs + L", respectively. On day 0, for "PBS" and "AIE NPs" groups. 100 μL of PBS and **FA-LSC NPs** (200 μg **LSC**) were separately injected into the Hela tumor-bearing mice through tail vein without subsequent laser irradiation. In case of "PBS + L" and "AIE NPs + L" groups, after intravenous injection 100 μL of PBS and **FA-LSC NPs** for 12 h, respectively, the tumor of mice each group were continuously irradiated with 808 nm laser (2 W cm^{-2}) for 10 min. After a variety of treatments, the mouse body weight and tumor volume were recorded every 2 days during 14-day study duration. The tumor volume was measured by a vernier caliper and calculated as $V = a \times b^2/2$ (a: tumor length; b: tumor width).

HE Analysis

Tumor and the major organs (heart, liver, spleen, lung and kidney) were dissected from mice. Paraffin-embedded sections were deparaffinized and hydrated. Hematoxylin

solution was added to cover the slides; after staining for 3 min, the slides were washed with saline to remove excess hematoxylin staining solution. The slides were immersed in the differentiation solution for 3 s. The slides were incubated with eosin for an additional 3 min, and then rinsed with saline. The nucleus was stained blue with hematoxylin, and the cytoplasm was stained red with eosin. The cells were observed using light microscopy.

Statistical analysis

All numeric data are expressed as mean ± s.d. unless otherwise indicated. For multiple comparisons, one-way analysis of variance (ANOVA) with Tukey's post hoc test was used. Statistical analysis was performed using GraphPad Prism 6.0. P values of less than 0.05 were considered significant. *P < 0.05, **P < 0.01, ***P < 0.001 and ****P < 0.0001.

2. Synthesis and characterization

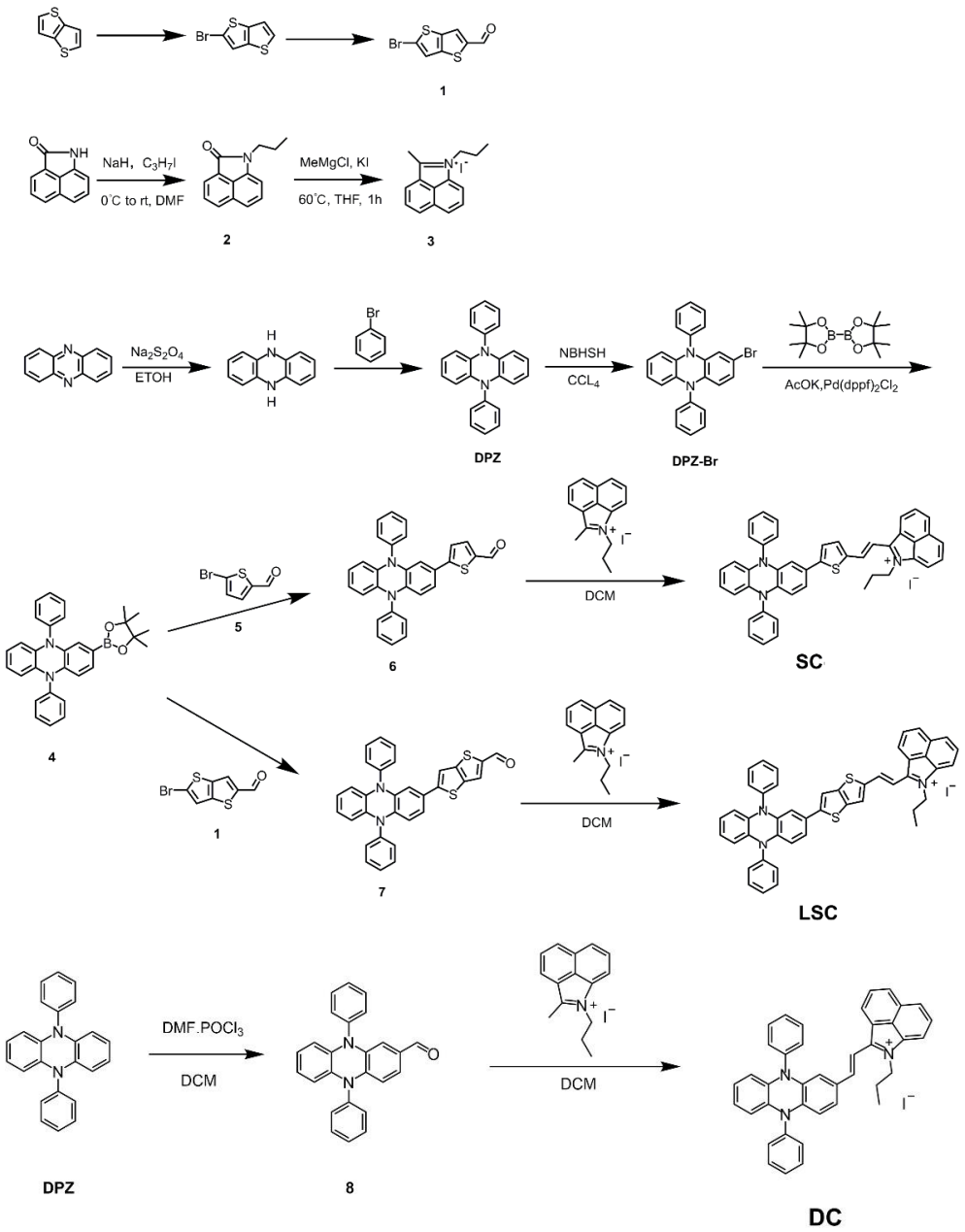

Scheme S1. The structures and synthetic routes of **DC**, **SC** and **LSC**.

General procedure for the synthesis of DC, SC and LSC

Synthetic route of 2: Intermediate compounds **2** and **3** were synthesized as previously reported in the literature. [3] Sodium hydride (NaH) (872 mg, 21.76 mmol) and Benz[c,d]indole-2(1H)-one (2.048 g, 7.26 mmol) were dissolved in anhydrous dimethylformamide (DMF) (20 mL) at in ice bath and agitated for 5 min. Proopyl iodide (1.9 g, 10.88 mmol) was added to the solution and agitated at 20 °C for 2 h. The reaction was terminated by adding water, and the crude product was extracted with ethyl acetate and purified by column chromatography (silica gel, ethyl acetate: petroleum ether =4:1), the product **1** was obtained as a yellow oil (1.3 g, 68%). ^{1}H NMR (400 MHz, DMSO - d_6) δ 8.19 (d, J = 8.0 Hz, 1H), 8.06 (d, J = 6.9 Hz, 1H), 7.81 (dd, J = 8.1, 7.0 Hz, 1H), 7.65 (d, J = 8.4 Hz, 1H), 7.55 (dd, J = 8.5, 7.0 Hz, 1H), 7.21 (d, J = 7.0 Hz, 1H), 3.87 (t, J = 7.1 Hz, 2H), 1.74 (p, J = 7.4 Hz, 2H), 0.91 (t, J = 7.4 Hz, 3H).

Synthetic route of 3: Methylmagnesium chloride (1.5 mL, 3.08 mmol) dropwise to solution **2** (300 mg, 1.18 mmol) in anhydrous tetrahydrofuran (THF) (2.0 mL) at an ice bath and subsequently transferred to 60 °C for 2 h. Add water (0.5 mL) and perchloric acid ($HClO_4$) (70%, 0.5 mL) were then successively added into the solution drop by drop after the solution was cooled to 0 °C. The product was then precipitated out by adding ice water (50 mL) and collected by vacuum filtration to give the product as a solid (270 mg, 92.5%). ^{1}H NMR (600 MHz, DMSO - d_6) δ 8.99 (d, J = 7.3 Hz, 1H), 8.80 (d, J = 8.2 Hz, 1H), 8.58 (d, J = 7.4 Hz, 1H), 8.45 (d, J = 8.2 Hz, 1H), 8.16 (t, J = 8.0 Hz, 1H), 7.99 (t, J = 7.8 Hz, 1H), 4.66 (t, J = 7.5 Hz, 2H), 3.25 (s, 3H), 1.96 (q, J = 7.3 Hz, 2H), 1.01 (t, J = 7.4 Hz, 3H). ^{13}C NMR (151 MHz, DMSO-d_6) δ 139.19, 135.81, 131.45, 130.25, 128.75, 122.51, 121.77, 48.60, 23.28, 14.72, 11.52.

Synthetic route of DPZ: Phenazine (1 g, 5.55 mmol) was dissolved in 20 mL of boiling ethanol and stirred for 1 h at 60 °C, sodium dithionite (12.3 g, 0.68 mmol) in 100 mL of water was added to the reaction system. After refluxing and stirring overnight, the solid was filtered, washed with water three times, and dried under vacuum to obtain a green solid product (1 g, yield: 98%). ^{1}H NMR (400 MHz, DMSO - d_6): δ 7.14 (d, 4H), 6.95 (t, 4H), 5.30 (s, 2H).

The above compound (500 mg, 2.75 mmol), bromobenzene (700 μL, 6.37 mmol), sodium tert-butoxide (750 mg, 7.8 mmol), palladium acetate (25 mg, 0.11 mmol), three tert-butyl phosphine (120 μL, 0.11 mmol) were added into a 100 mL three-necked flask. Then the air was pumped out, 5 mL of toluene was injected and heated at 95 °C overnight. After the reaction, the system was cooled to room temperature, washed three times with water, extracted with toluene, and dried with anhydrous sodium sulfate. The solvent was removed by vacuum distillation, then purified by column chromatography to give a yellow-green crystal **DPZ** (600 mg, yield: 64%). ^{1}H NMR (400 MHz, DMSO - d_6): δ 8.22 (d, 2H), 8.15 (d, 2H), 7.81 (d, 2H), 7.63 (t, 2H), 7.58 (d, 2H), 7.50 (m, 4H), 7.14 (m, 4H), 6.95 (t, 4H).

Synthetic route of DPZ-Br: A mixture of a compound **DPZ** (800 mg, 2.40 mmol) and NBS (426 mg, 2.40 mmol) dissolved in CCl_4, was heated to reflux for 2 h. After colling at r.t., add saturated sodium bicarbonate solution and stir for 15 min. Then CH_2Cl_2 (200 mL) and water (50 mL) was added. The organic layer was separated, washed with water (3×50 mL) and dried over sodium sulfate. The crude material was purified by column chromatography using hexane and evaporation of the solvent gave the yellow solid (234 mg, 23.6%). ^{1}H NMR (600 MHz, Benzene - d_6) δ 7.13 (d, J = 7.4 Hz, 2H), 7.07 (t, J = 8.4 Hz, 4H), 7.02 (dt, J = 7.4, 3.8 Hz, 3H), 6.96 (d, J = 7.6 Hz, 1H), 6.39 (d, J = 8.9 Hz, 1H), 6.23 (q, J = 6.7 Hz, 2H), 6.04 (d, J = 2.2 Hz, 1H), 5.73 (t, J = 9.9 Hz, 2H), 5.50 (d, J = 8.5 Hz, 1H). ^{13}C NMR (151 MHz, Benzene - d_6) δ 140.25, 139.72, 138.64, 136.69, 136.44, 131.61, 131.56, 131.31, 131.08, 128.54, 128.36, 123.72, 121.90, 121.64, 115.51, 114.04, 113.86, 113.43, 113.18. HRMS (ESI, m/z): calculated for $C_{24}H_{17}N_2Br$: 412.0575, found: 412.0576.

Synthetic route of 4: A mixture of **DPZ-Br** (100 mg, 0.24 mmol), potassium acetate (71 mg, 0.73 mmol), [1,1' -bis (diphenylphosphine) ferrocene] palladium dichloride (85 mg, 0.12 mmol) and bis (pinacol) diboron (123 mg, 0.48 mmol) was vacuumed three times and filled with N_2. Then 200 mL dioxane was added into the mixture and stirred at 90 ℃ for 5 h. After the reaction is complete, the solids are removed by filtration and the concentrated filtrate is evaporated. The crude material was purified by column

chromatography using hexane and evaporation of the solvent gave the yellow solid (48 mg, 43%). ^{1}H NMR (400 MHz, Benzene - d_6) δ 7.36 (dd, J = 7.9, 1.4 Hz, 1H), 7.22 – 7.19 (m, 2H), 7.12 – 7.04 (m, 6H), 6.99 (dt, J = 7.5, 3.0 Hz, 1H), 6.96 – 6.92 (m, 1H), 6.67 (d, J = 1.4 Hz, 1H), 6.23 (tt, J = 7.5, 5.6 Hz, 2H), 5.92 (d, J = 8.0 Hz, 1H), 5.76 (ddd, J = 7.4, 5.4, 2.3 Hz, 2H), 0.95 (s, 12H). ^{13}C NMR (151 MHz, Benzene - d_6) δ 139.39, 139.19, 139.04, 136.39, 135.55, 135.40, 130.33, 130.25, 130.21, 128.94, 120.70, 119.97, 117.43, 112.12, 112.02, 111.42, 82.05, 23.60. HRMS (ESI, m/z): calculated for $C_{30}H_{29}N_2BO_2$: 460.2322, found: 460.2325.

Synthetic route of 6: A 100 mL round-bottomed flask was charged with compound **4** (460 mg, 1 mmol), bromo-thiophene (228 mg, 1.2mmol), K_2CO_3 (405 mg, 3.0 mmol) and DMF/H_2O (0.5 M, 1:1 v/v) to an oven dried two-necked round bottomed flask equipped with a magnetic stir bar. Degas the suspension by nitrogen bubbling. Bubble the suspension over 15 min. Add $Pd(OAc)_2$ (6.6 mg, 0.03 mmol), PPh_3 (15.4 mg, 0.06 mmol, 6.0 mol%) to the solution. Heat the mixture under reflux with stirring overnight. Cool the reaction mixture to room temperature. Extract the reaction mixture with EtOAc three times. Wash the combined organic layer with brine. Dry combined organic layer over $MgSO_4$. Remove the solvent by evaporation. Purify the reside by flash column chromatography on silica gel (hexane/ethyl acetate = 20:1, 5:1 to 4:1). ^{1}H NMR (600 MHz, Acetone - d_6) δ 9.78 (s, 1H), 7.76 (qd, J = 8.0, 5.6, 4.0 Hz, 6H), 7.62 – 7.58 (m, 2H), 7.49 (d, J = 7.6 Hz, 2H), 7.46 (d, J = 7.8 Hz, 2H), 7.07 – 7.01 (m, 1H), 6.74 (s, 1H), 6.31 (s, 1H), 5.87 (s, 1H), 5.66 – 5.58 (m, 3H). ^{13}C NMR (151 MHz, Acetone-d_6) δ 205.13, 182.37, 153.56, 140.73, 139.62, 139.51, 138.17, 137.58, 137.24, 135.99, 135.63, 132.28, 131.76, 131.63, 130.92, 130.85, 128.84, 128.78, 125.57, 123.23, 122.28, 121.57, 121.20, 119.51, 112.83, 112.72, 112.44, 109.49. HRMS (ESI, m/z): calculated for $C_{29}H_{20}N_2OS$: 444.1296, found: 444.1298.

Synthetic route of SC: A mixture of a compound **6** (60 mg 0.135mmol) and compound **3** (100 mg, 0.26 mmol) in 6 mL of ethanol at 95°C were refluxed for 12 h in a 100 mL round bottom flask, and then cooled to room temperature. The organic phase was dried with Na_2SO_4 and evaporated in vacuo. The crude product was subjected to column

chromatography on silica gel with MeOH/DCM = 1:100 to afford **SC** as a dark purple solid product (49 mg, yield: 50%). ^{1}H NMR (600 MHz, DMSO - d_6) δ 9.20 (d, J = 7.4 Hz, 1H), 8.90 (d, J = 15.1 Hz, 1H), 8.61 (d, J = 8.0 Hz, 1H), 8.22 (d, J = 8.5 Hz, 2H), 8.12 – 8.06 (m, 2H), 7.89 (t, J = 7.8 Hz, 1H), 7.77 (dt, J = 25.6, 7.6 Hz, 4H), 7.66 – 7.60 (m, 2H), 7.56 – 7.46 (m, 5H), 7.28 (s, 1H), 6.93 – 6.87 (m, 1H), 6.39 – 6.31 (m, 2H), 5.78 (s, 1H), 5.55 (q, J = 8.7 Hz, 3H), 4.66 (t, J = 7.4 Hz, 2H), 1.89 (q, J = 7.4 Hz, 2H), 0.99 (t, J = 7.4 Hz, 3H). ^{13}C NMR (151 MHz, DMSO - d_6) δ 207.29, 167.45, 132.06, 130.98, 129.72, 129.60, 129.42, 129.13, 128.02, 123.65, 110.93, 106.48, 100.91, 98.44, 95.28, 67.87, 55.40, 48.95, 23.71, 11.28. HRMS (ESI, m/z): calculated for $C_{44}H_{34}N_3S^+$: 636.2468, found: 636.2472.

Synthetic route of 7: A 100 mL round-bottomed flask was charged with compound **4** (460 mg, 1 mmol), compound **1** (294 mg, 1.2mmol), K_2CO_3 (405 mg, 3.0 mmol) and DMF/H_2O (0.5 M, 1:1 v/v) to an oven dried two-necked round bottomed flask equipped with a magnetic stir bar. Degas the suspension by nitrogen bubbling. Bubble the suspension over 15 min. Add $Pd(OAc)_2$ (6.6 mg, 0.03 mmol), PPh_3 (15.4 mg, 0.06 mmol, 6.0 mol%) to the solution. Heat the mixture under reflux with stirring overnight. Cool the reaction mixture to room temperature. Extract the reaction mixture with EtOAc three times. Wash the combined organic layer with brine. Dry combined organic layer over $MgSO_4$. Remove the solvent by evaporation. Purify the reside by flash column chromatography on silica gel (hexane/ethyl acetate = 20:1). ^{1}H NMR (400 MHz, Acetone - d_6) δ 9.93 (s, 1H), 8.15 (s, 1H), 7.77 (d, J = 7.8 Hz, 4H), 7.66 – 7.54 (m, 4H), 7.53 – 7.44 (m, 5H), 7.26 (dd, J = 8.7, 2.6 Hz, 1H), 5.90 – 5.85 (m, 1H), 5.63 (s, 3H). ^{13}C NMR (151 MHz, Acetone - d_6) δ 183.11, 131.72, 131.59, 130.86, 130.80, 130.07, 128.78, 128.72, 124.54, 124.00, 121.45, 121.15, 119.16, 112.76, 112.68, 112.66, 112.48, 109.37, 78.34, 78.11, 77.90. HRMS (ESI, m/z): calculated for $C_{31}H_{20}N_2S_2O$: 500.1017, found: 500.1015.

Synthetic route of LSC: A mixture of a compound **7** (60 mg 0.12mmol) and compound **3** (100 mg, 0.26 mmol) in 6 mL of ethanol at 95°C were refluxed for 12 h in a 100 mL round bottom flask, and then cooled to room temperature. The organic phase was dried

with Na_2SO_4 and evaporated in vacuo. The crude product was subjected to column chromatography on silica gel with MeOH/DCM = 1:100 to afford **LSC** as a dark purple solid product (39 mg, yield: 47%). ^{1}H NMR (600 MHz, DMSO - d_6) δ 9.19 (d, J = 7.4 Hz, 1H), 8.95 (d, J = 19.8 Hz, 1H), 8.57 (d, J = 8.0 Hz, 1H), 8.31 (d, J = 6.9 Hz, 1H), 8.19 (t, J = 8.7 Hz, 2H), 8.07 (t, J = 7.7 Hz, 1H), 7.85 (t, J = 7.7 Hz, 2H), 7.76 (s, 2H), 7.62 (dt, J = 29.6, 7.3 Hz, 3H), 7.54 – 7.13 (m, 6H), 6.85 – 6.61 (m, 1H), 6.40 (d, J = 87.6 Hz, 2H), 5.62 (d, J = 6.2 Hz, 4H), 4.66 (t, J = 7.3 Hz, 2H), 1.90 (q, J = 7.4 Hz, 2H), 1.02 (t, J = 7.4 Hz, 3H). ^{13}C NMR (151 MHz, DMSO - d_6) δ 136.29, 134.19, 132.39, 131.08, 130.22, 129.79, 129.46, 129.29, 127.96, 123.59, 119.23, 115.68, 79.67, 79.46, 79.24, 60.69, 23.64, 11.59. HRMS (ESI, m/z): calculated for $C_{46}H_{34}N_3S_2^+$: 692.2189, found: 692.2188.

Synthetic route of 8: To a 100 mL round bottom flask, phosphorus oxychloride (4.5 mL) was slowly added into ultra-dry DMF (4.5 mL) in an ice bath. The reaction was stirred for 5 min, then moved to room temperature, and stirred for otherwise 30 min, **DPZ** (225 mg, 0.675 mmol) dissolved in 4 mL of ultra-dry DCM was added to the system gently, then the system was stirred at room temperature for 2h. After the reaction was completed, it was quenched with saturated sodium bicarbonate solution under ice bath conditions. The organic phase was extracted by DCM, dried with anhydrous sodium sulfate, and purified by column chromatography to obtain an orange solid product (200 mg, 82%). ^{1}H NMR (400 MHz, DMSO - d_6): δ 9.88 (s, 1H), 7.52 (s, 1H), 7.33 (d, 1H), 7.24 (t, 4H), 7.14 (d, 2H), 7.08 (d, 4H), 7.00 (t, 2H), 6.95 (m, 3H).

Synthetic route of DC: 8 (50 mg, 0.138 mmol), **3** (36.9 mg, 0.138 mmol) in 5 mL of ethanol at 95°C were refluxed for 12 h in a 100 mL round bottom flask, and then cooled to room temperature. The organic phase was dried with Na_2SO_4 and evaporated in vacuo. The crude product was subjected to column chromatography on silica gel with MeOH/DCM = 1:100 to afford **DC** as solid product (42 mg, yield: 49%). ^{1}H NMR (400 MHz, DMSO - d_6) δ 8.99 (d, J = 7.5 Hz, 1H), 8.50 (d, J = 8.1 Hz, 1H), 8.32 (d, J = 15.3 Hz, 1H), 8.08 (dd, J = 15.9, 7.8 Hz, 2H), 8.00 (t, J = 7.8 Hz, 1H), 7.86 – 7.75 (m, 5H), 7.70 – 7.64 (m, 2H), 7.60 – 7.52 (m, 4H), 7.39 (dd, J = 8.6, 1.6 Hz, 1H), 6.84 (d, J =

15.3 Hz, 1H), 6.55 – 6.49 (m, 1H), 6.46 – 6.39 (m, 1H), 5.99 (d, J = 1.9 Hz, 1H), 5.74 – 5.61 (m, 3H), 4.38 (t, J = 7.3 Hz, 2H), 1.71 (p, J = 7.3 Hz, 2H), 0.91 (t, J = 7.4 Hz, 3H). ^{13}C NMR (151 MHz, DMSO - d_6) δ 158.19, 150.03, 143.55, 139.63, 138.13, 137.29, 136.92, 135.76, 134.71, 133.18, 132.70, 132.08, 131.89, 130.52, 130.34, 129.72, 129.56, 129.24, 128.95, 127.72, 127.28, 124.11, 123.27, 121.48, 115.83, 114.44, 112.87, 112.62, 109.01, 46.21, 39.50, 22.57, 11.15. HRMS (ESI, m/z): calculated for $C_{40}H_{32}N_3^+$: 554.2519, found: 554.2598.

NMR and HRMS spectra of compounds

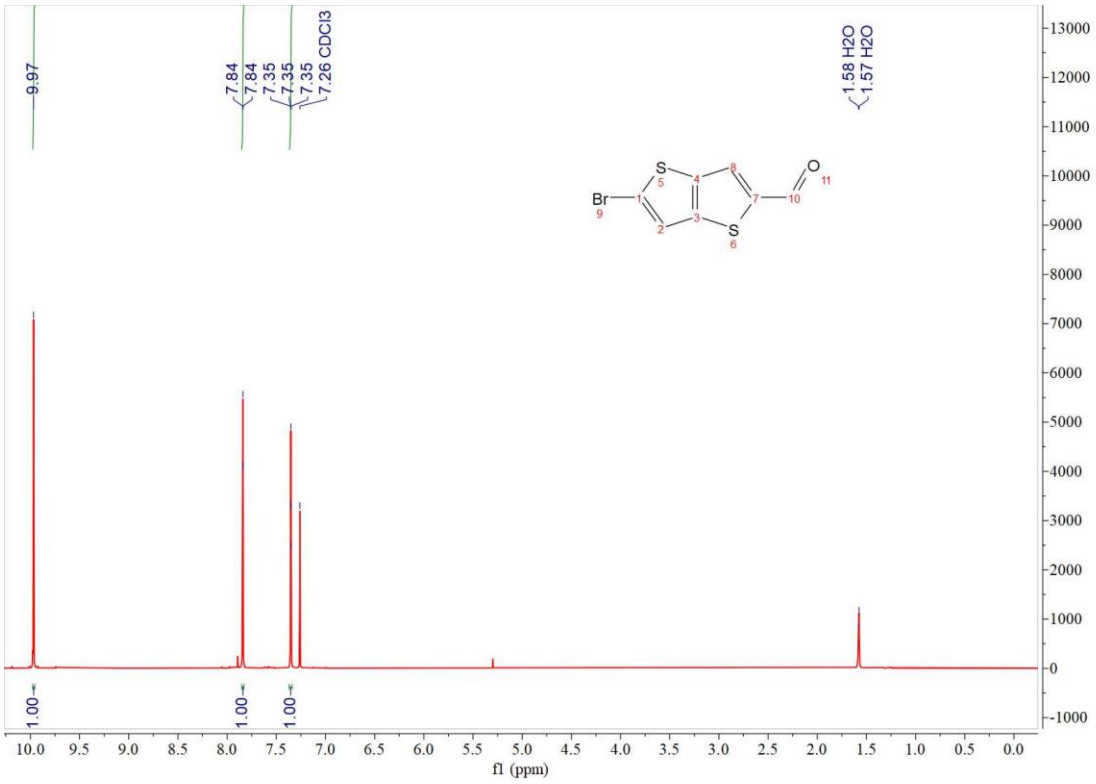

Figure S1. [1]H NMR spectrum of **1**.

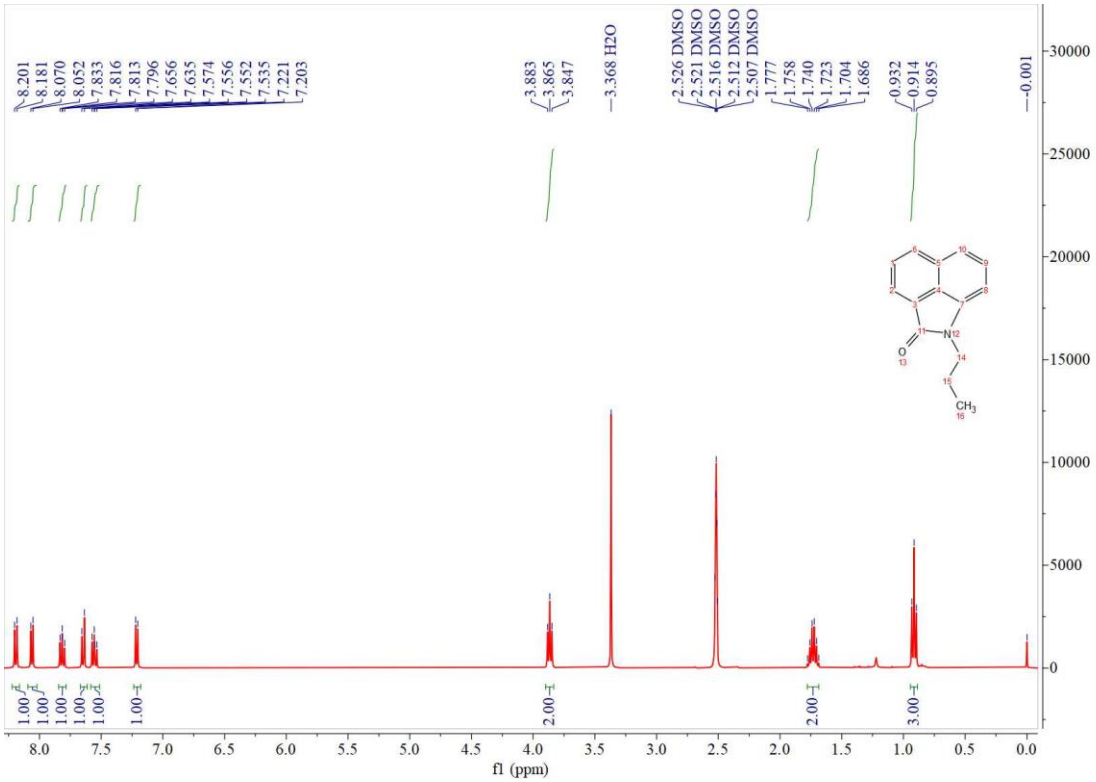

Figure S2. [1]H NMR spectrum of **2**.

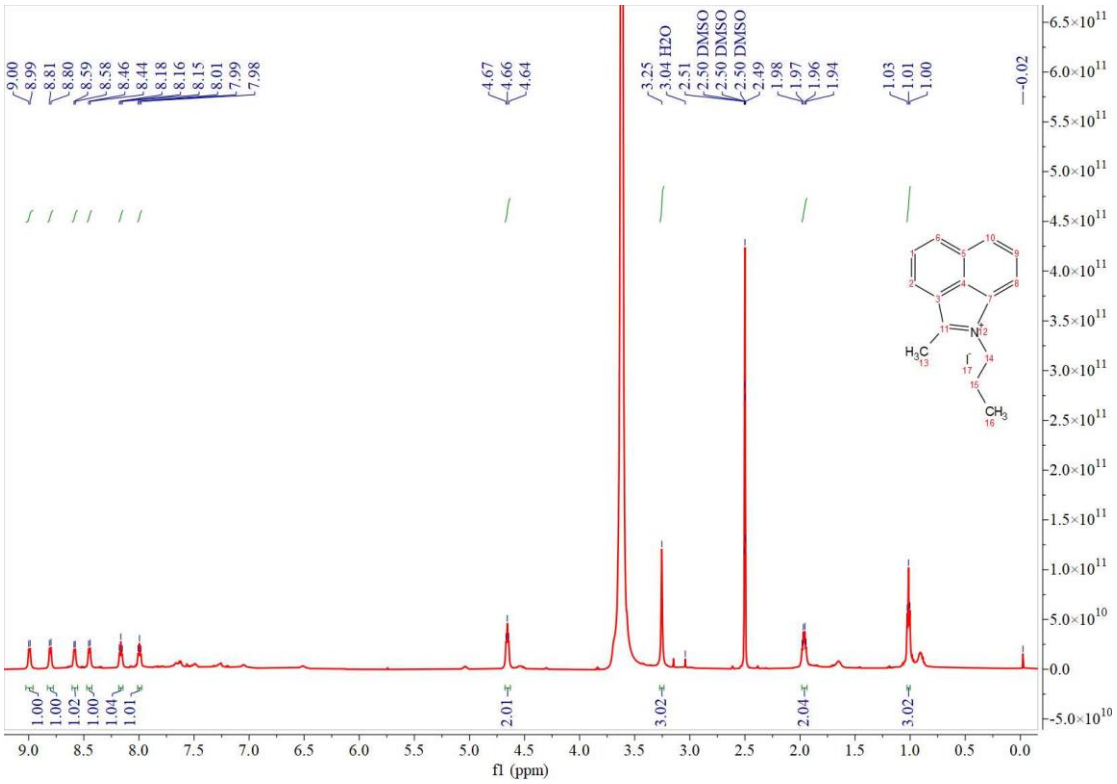

Figure S3. ^{1}H NMR spectrum of **3**.

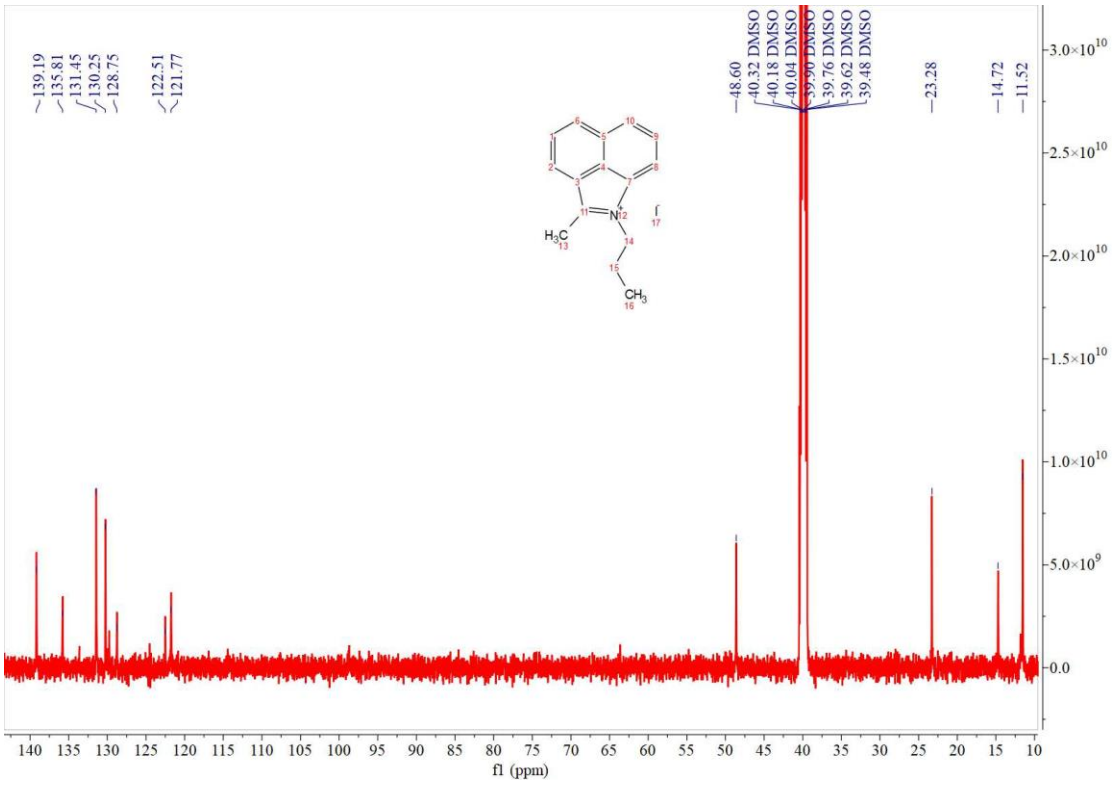

Figure S4. ^{13}C NMR spectrum of **3**.

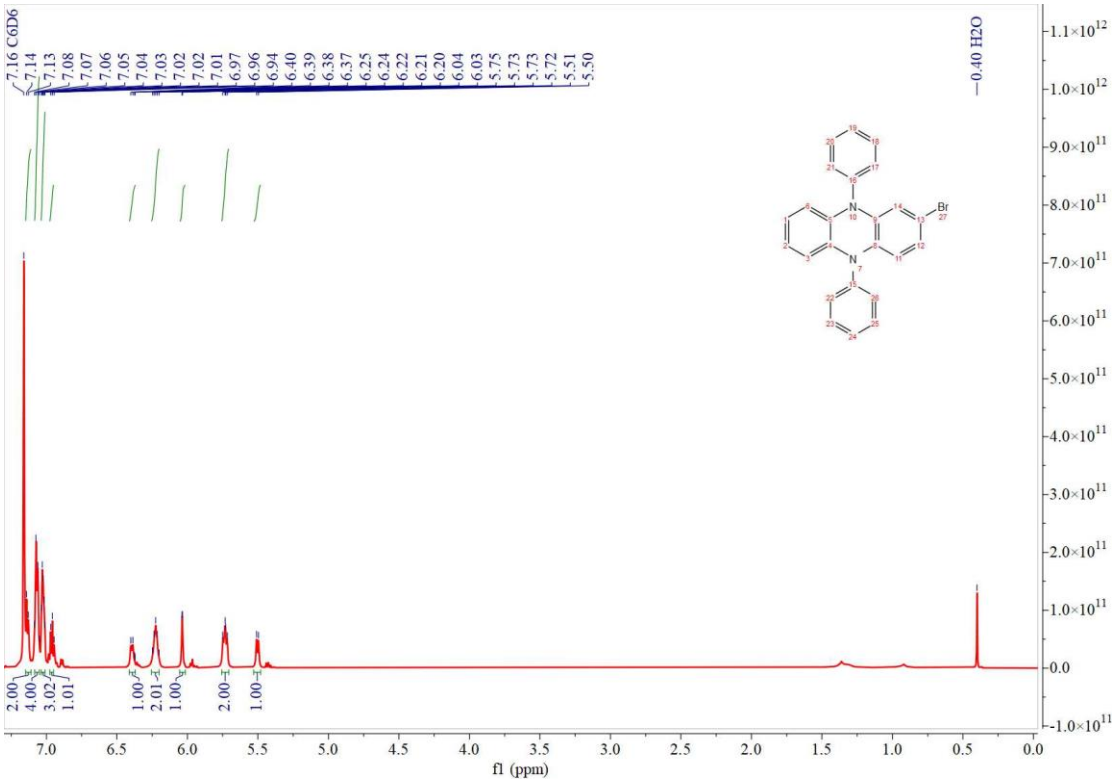

Figure S5. [1]H NMR spectrum of **DPZ-Br**.

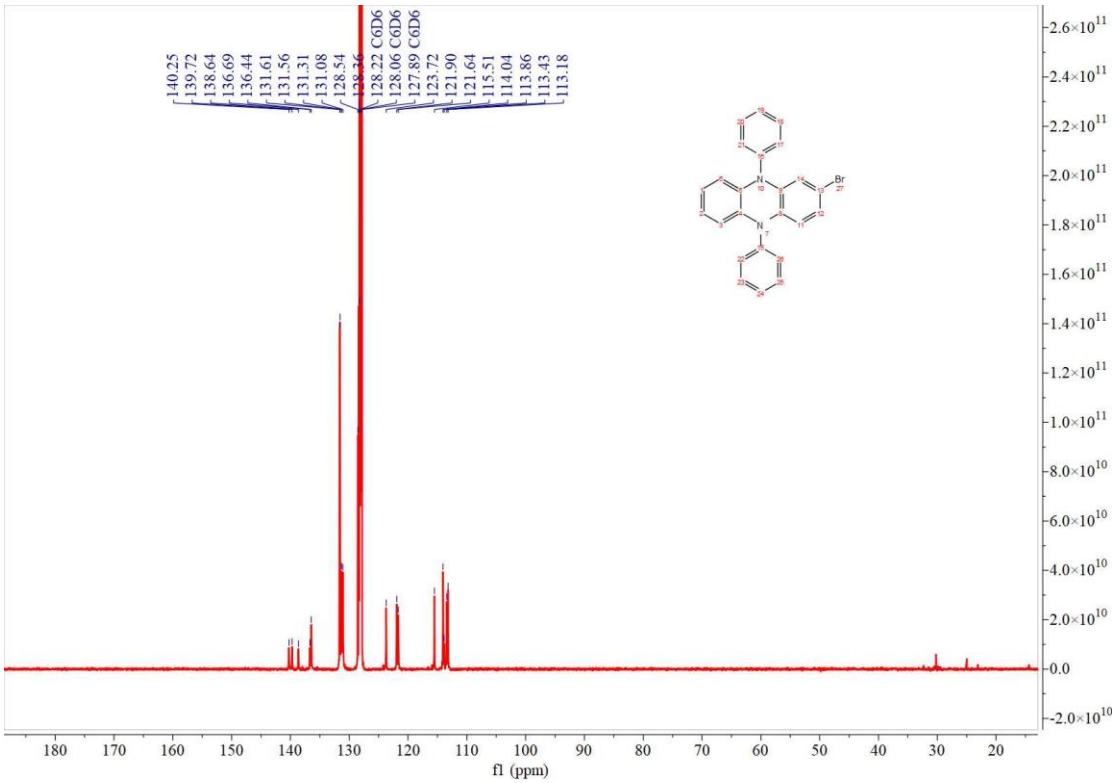

Figure S6. [13]C NMR spectrum of **DPZ-Br**.

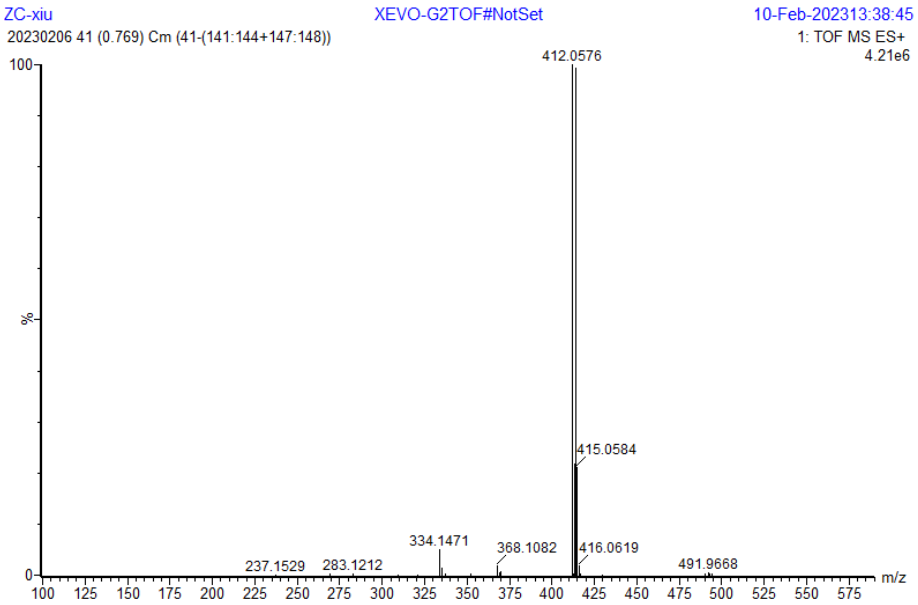

Figure S7. HRMS spectrum of **DPZ-Br.**

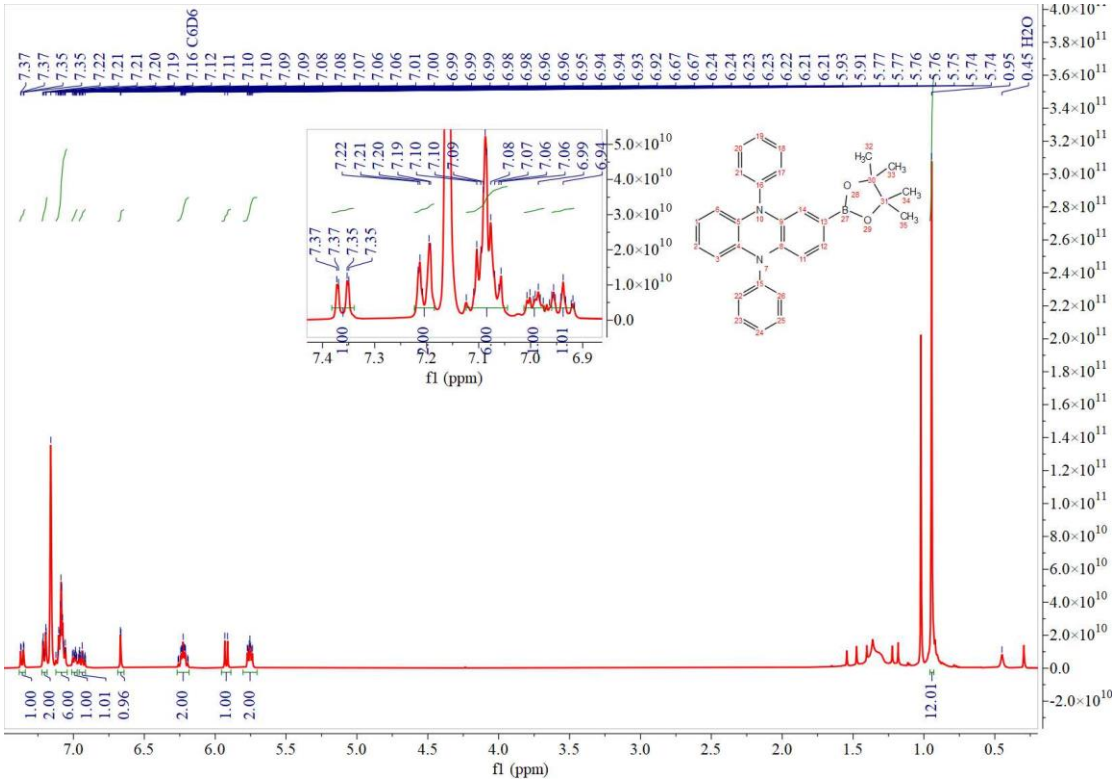

Figure S8. ^{1}H NMR spectrum of **4**.

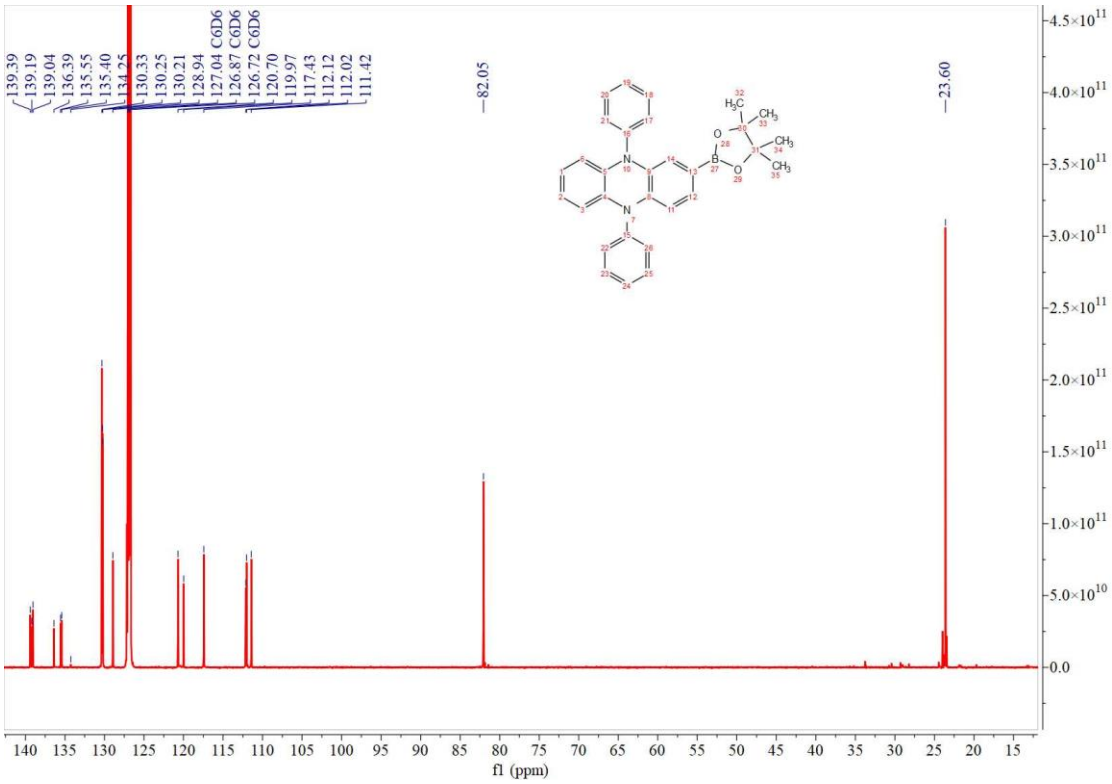

Figure S9. ^{13}C NMR spectrum of **4**.

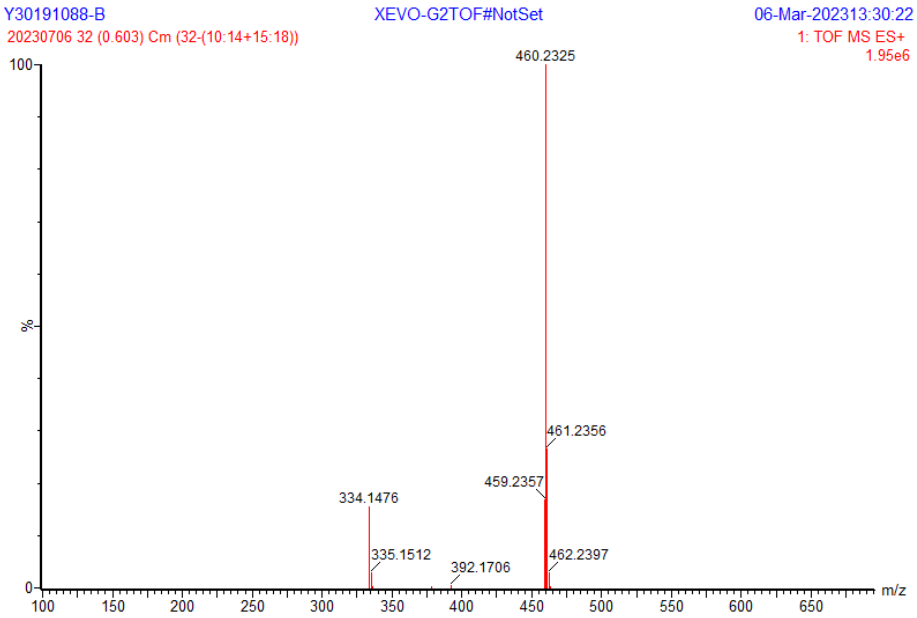

Figure S10. HRMS spectrum of **4**.

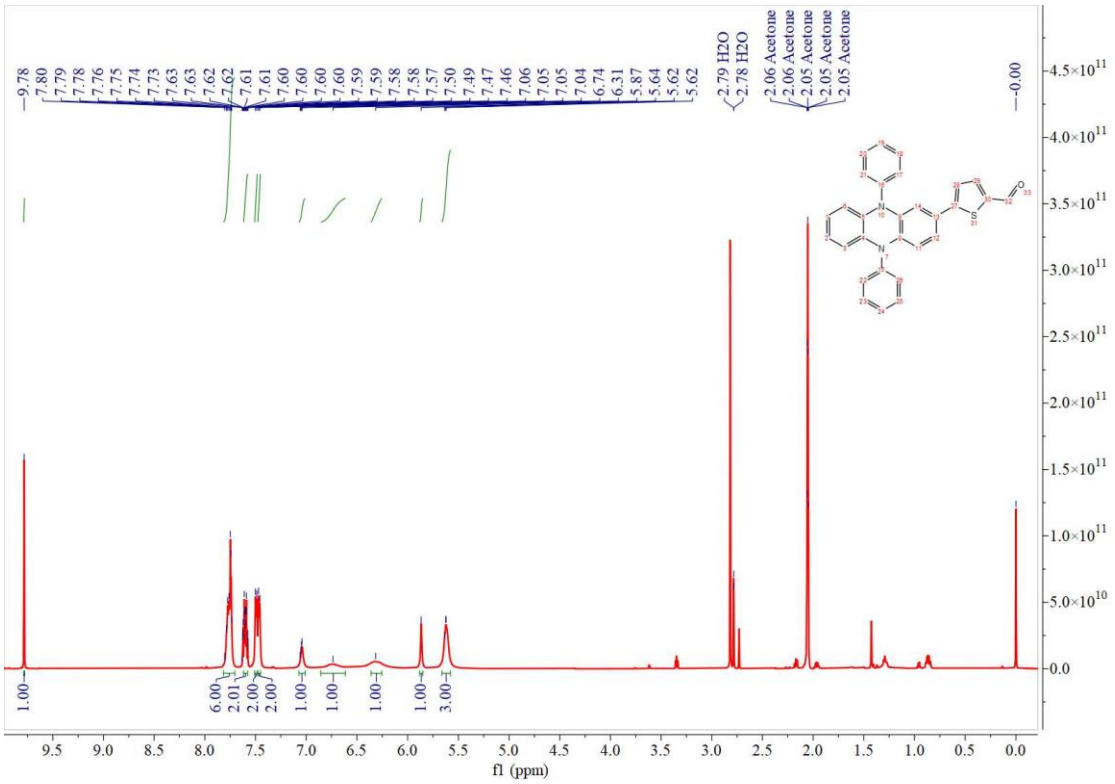

Figure S11. ^{1}H NMR spectrum of **6**.

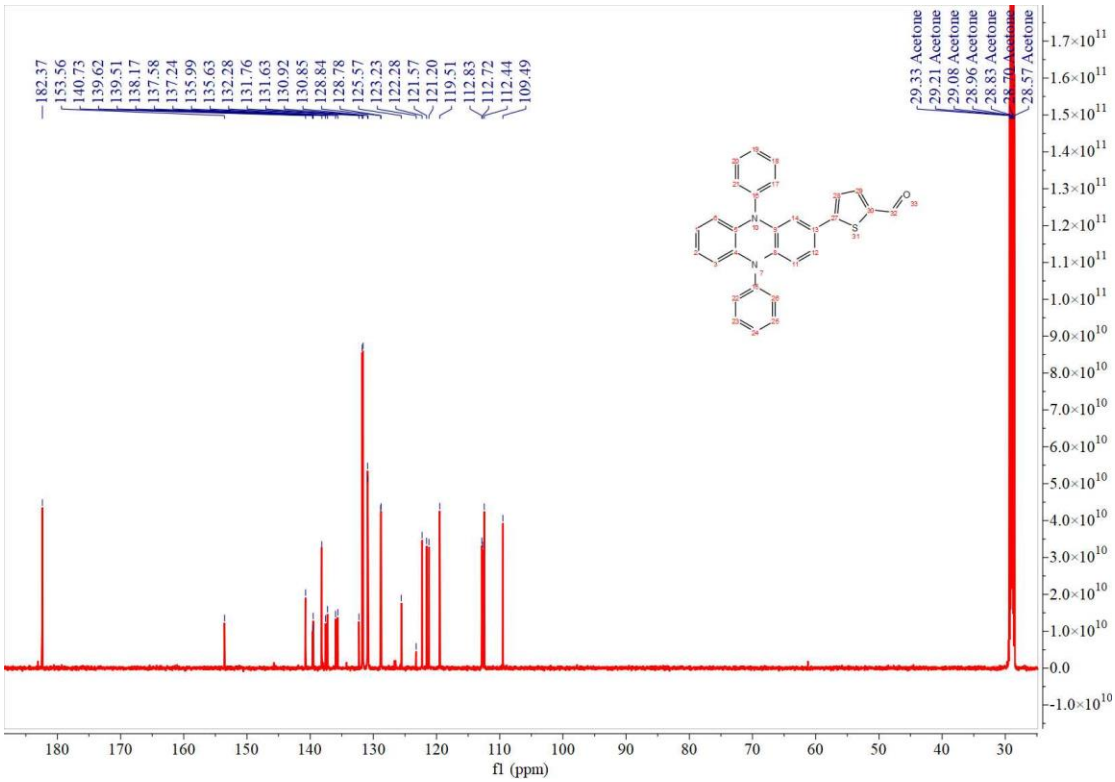

Figure S12. ^{13}C NMR spectrum of **6**.

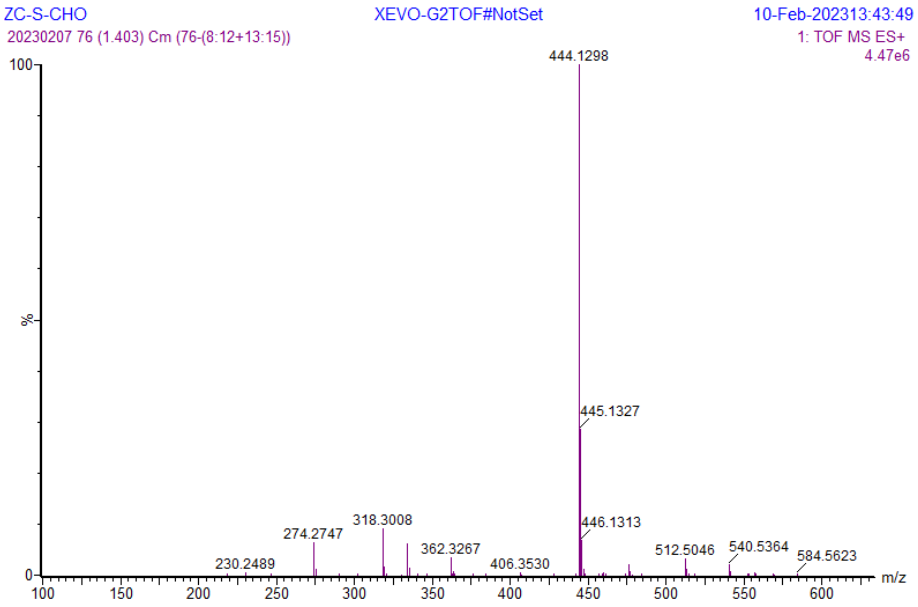

Figure S13. HRMS spectrum of **6**.

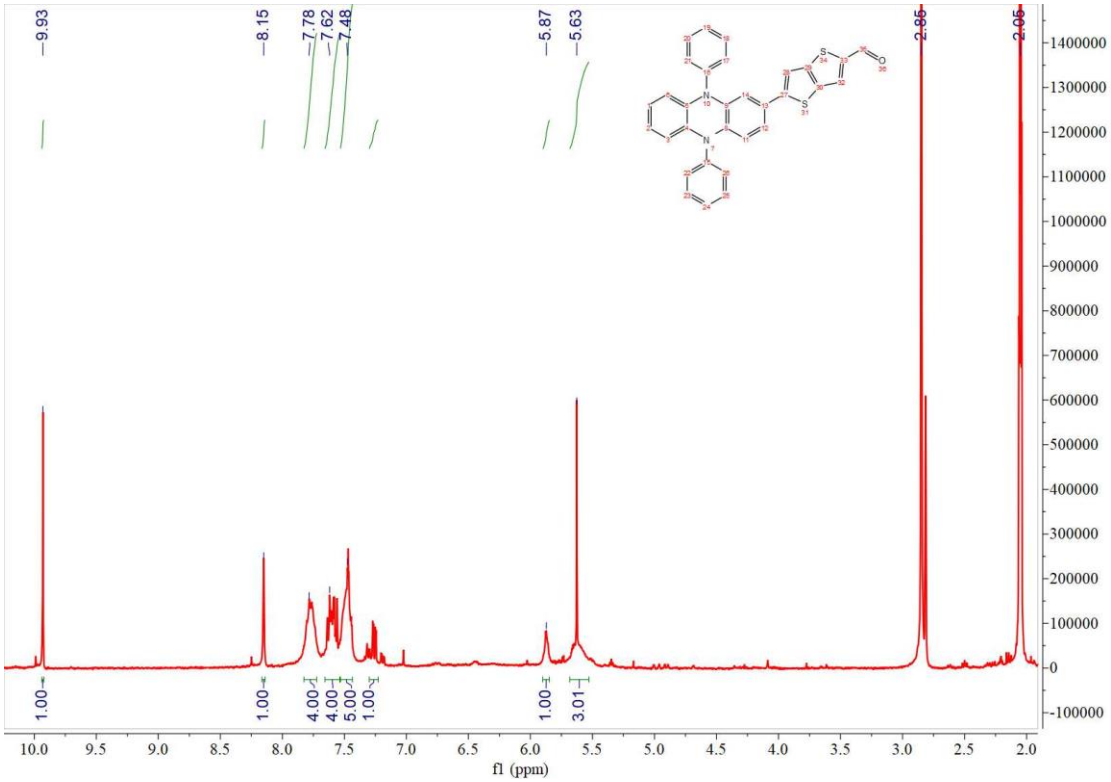

Figure S14. ^{1}H NMR spectrum of **7**.

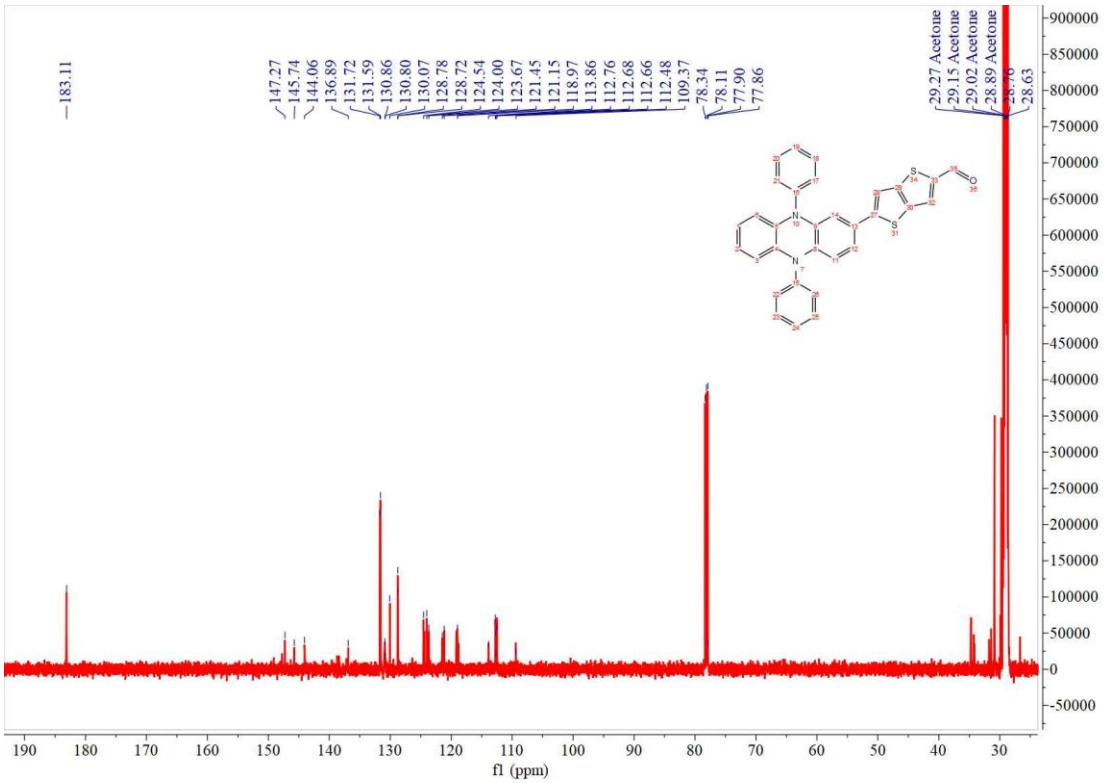

Figure S15. ^{13}C NMR spectrum of **7**.

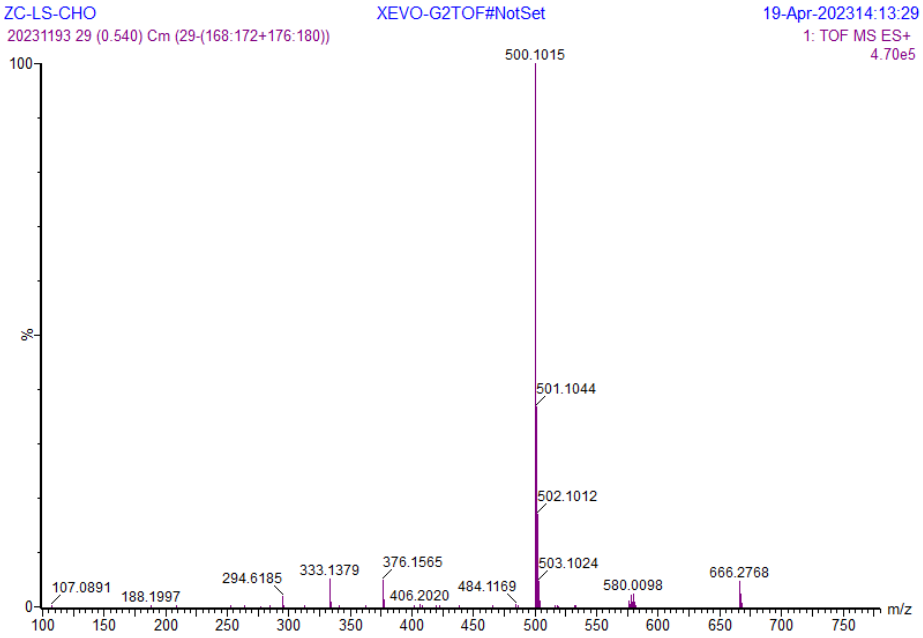

Figure S16. HRMS spectrum of **7**.

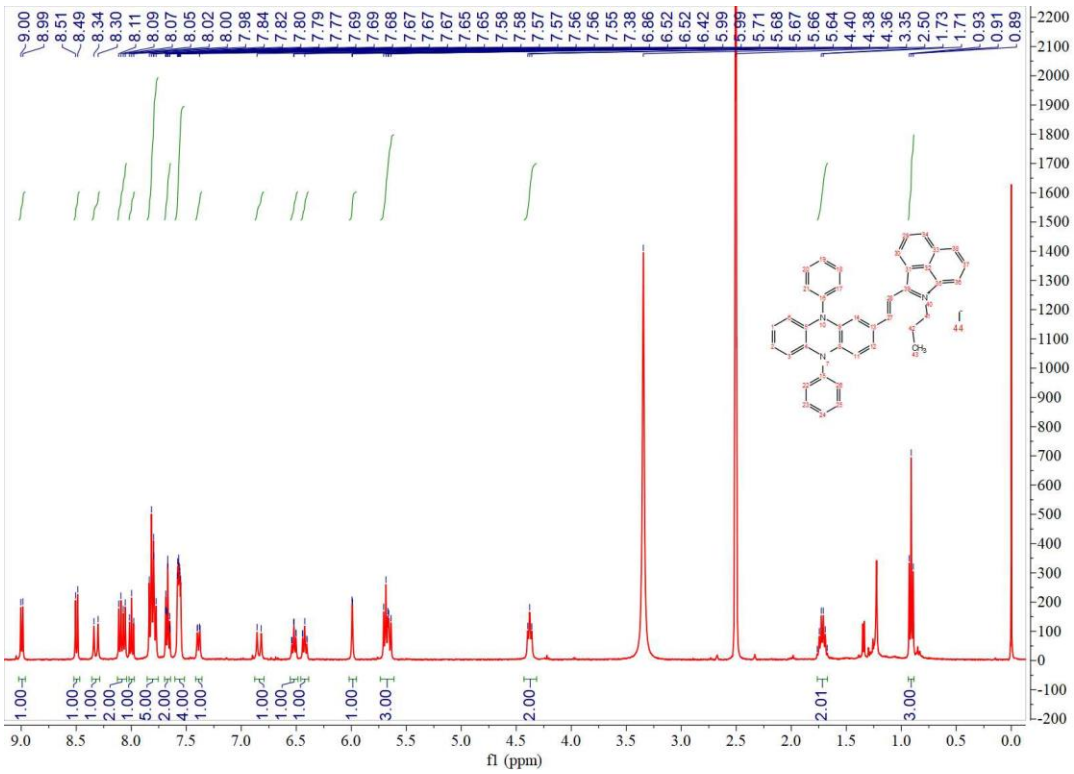

Figure S17: ^{1}H NMR spectrum of **DC**.

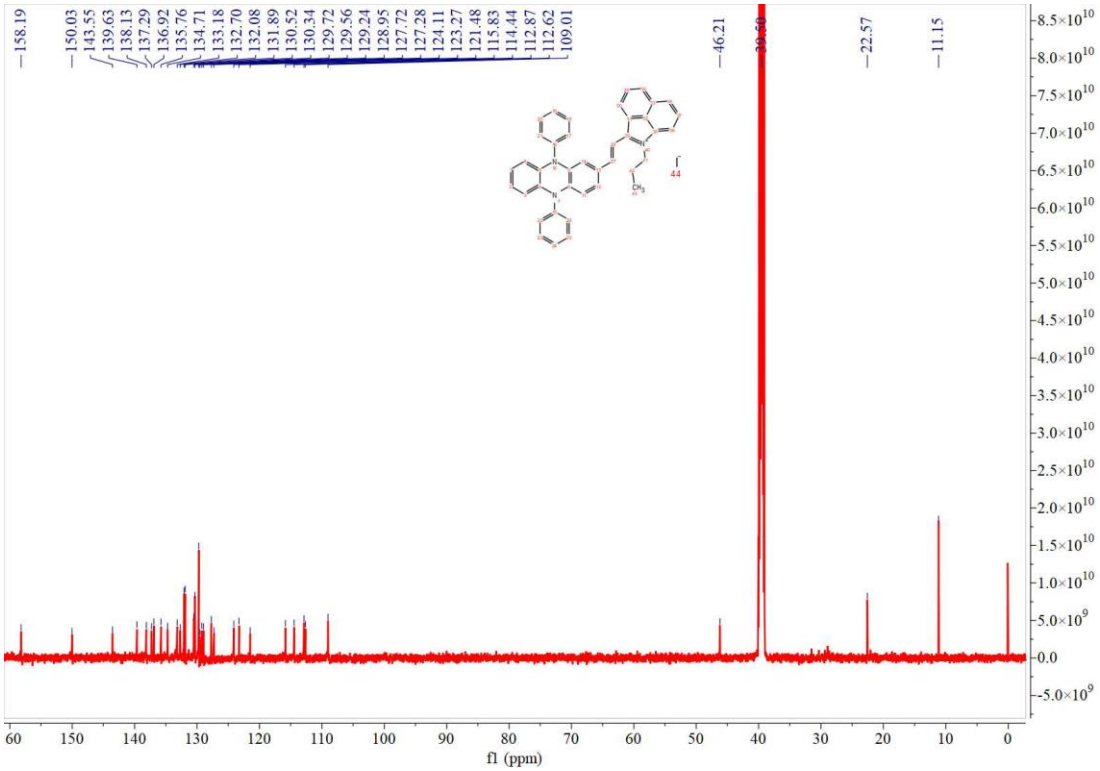

Figure S18. ^{13}C NMR spectrum of **DC**.

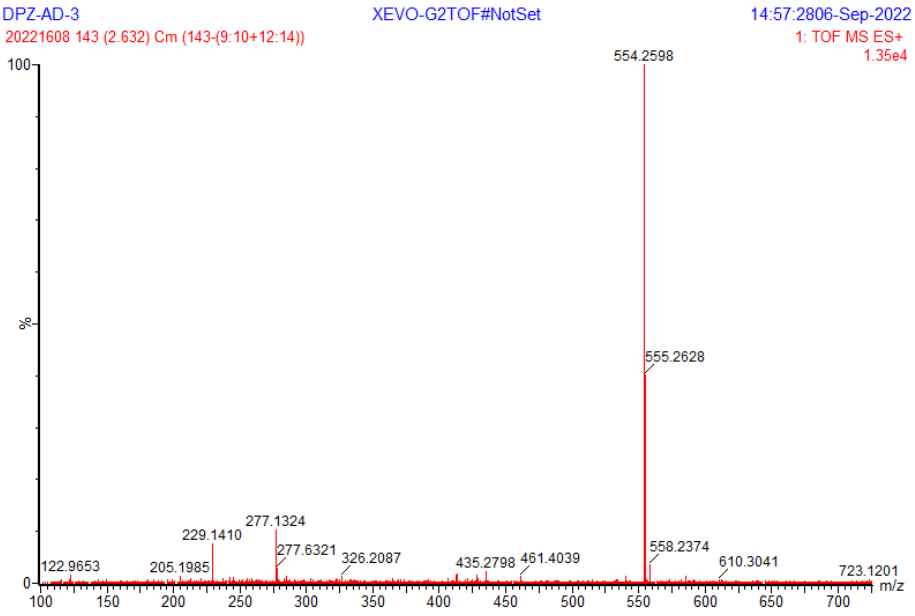

Figure S19. HRMS spectrum of **DC**.

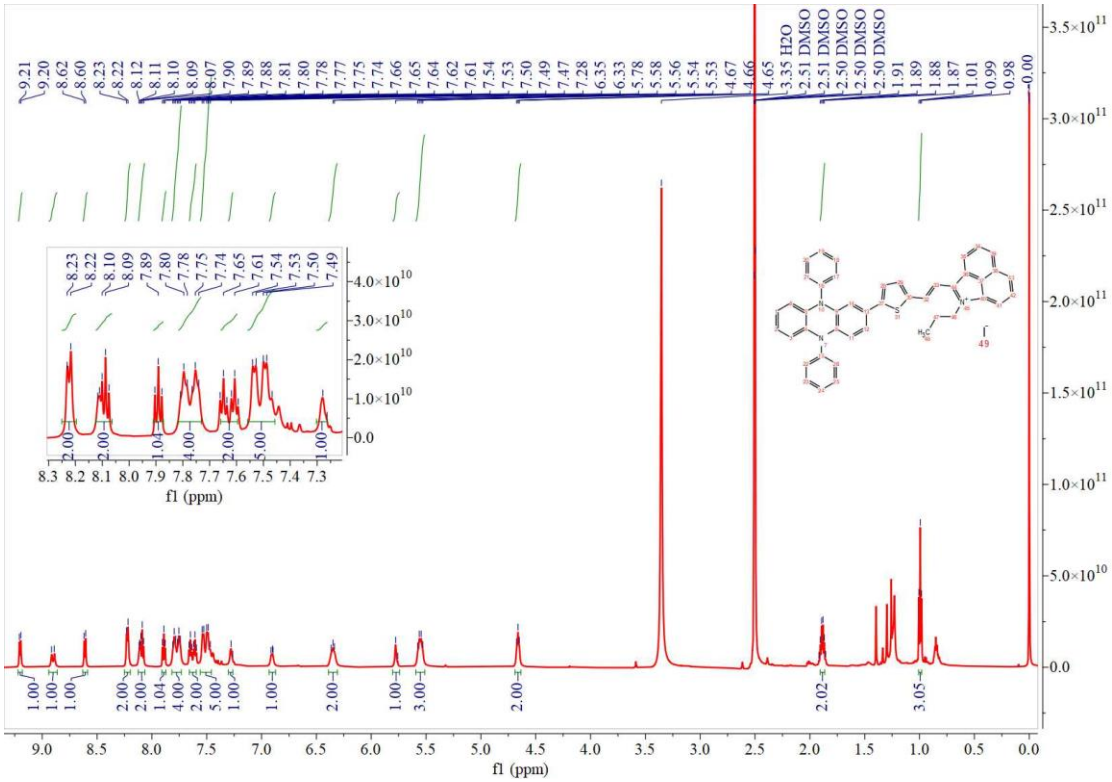

Figure S20: ^{1}H NMR spectrum of **SC**.

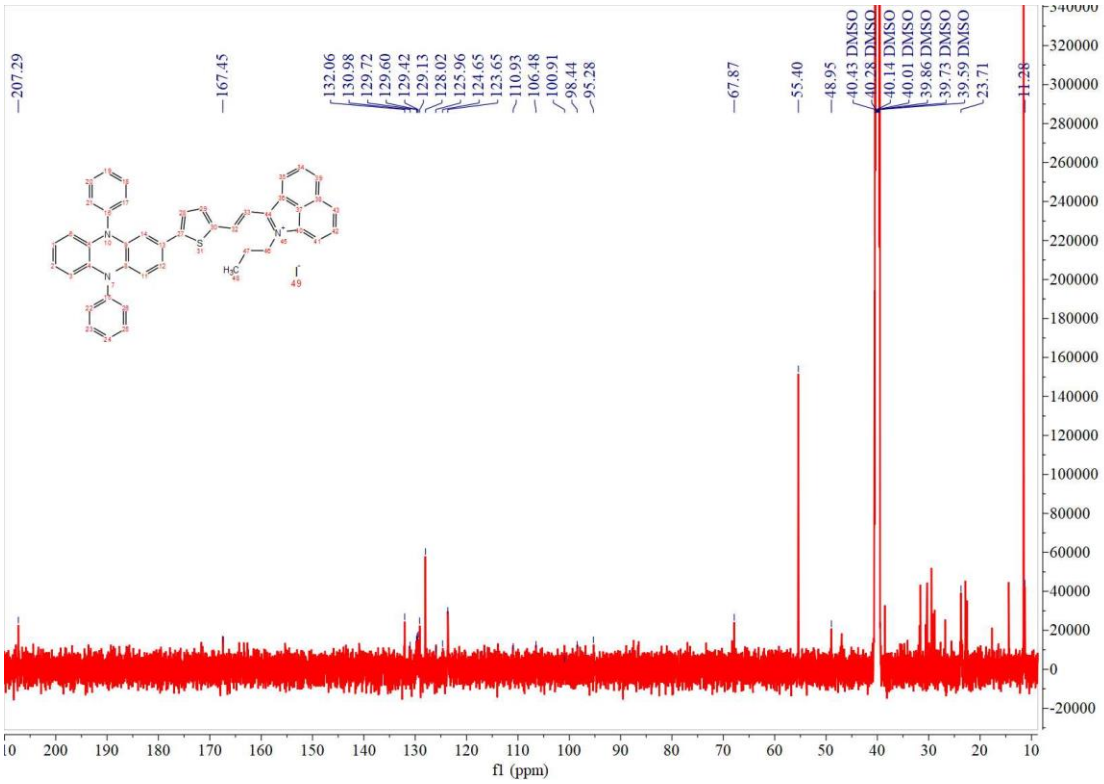

Figure S21. ^{13}C NMR spectrum of **SC**.

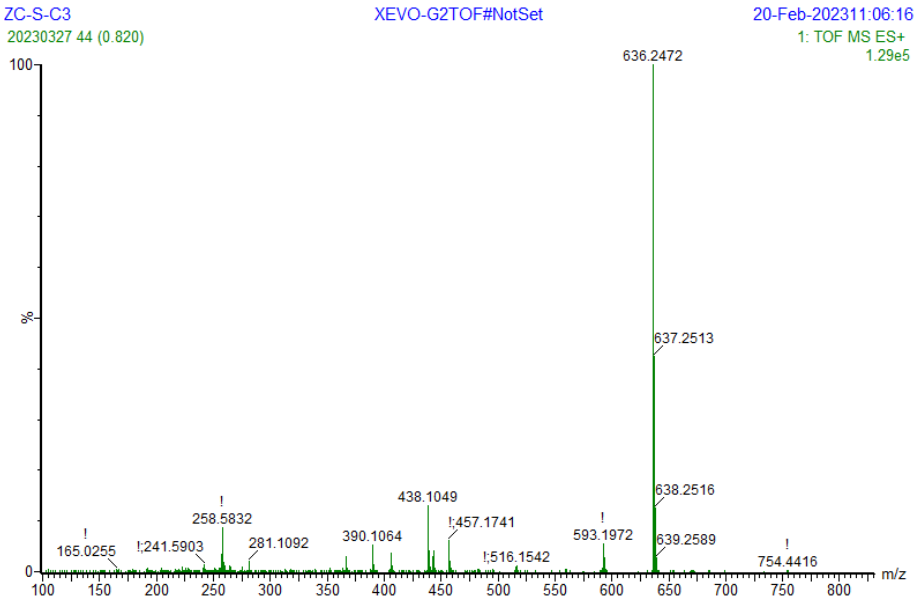

Figure S22. HRMS spectrum of **SC**.

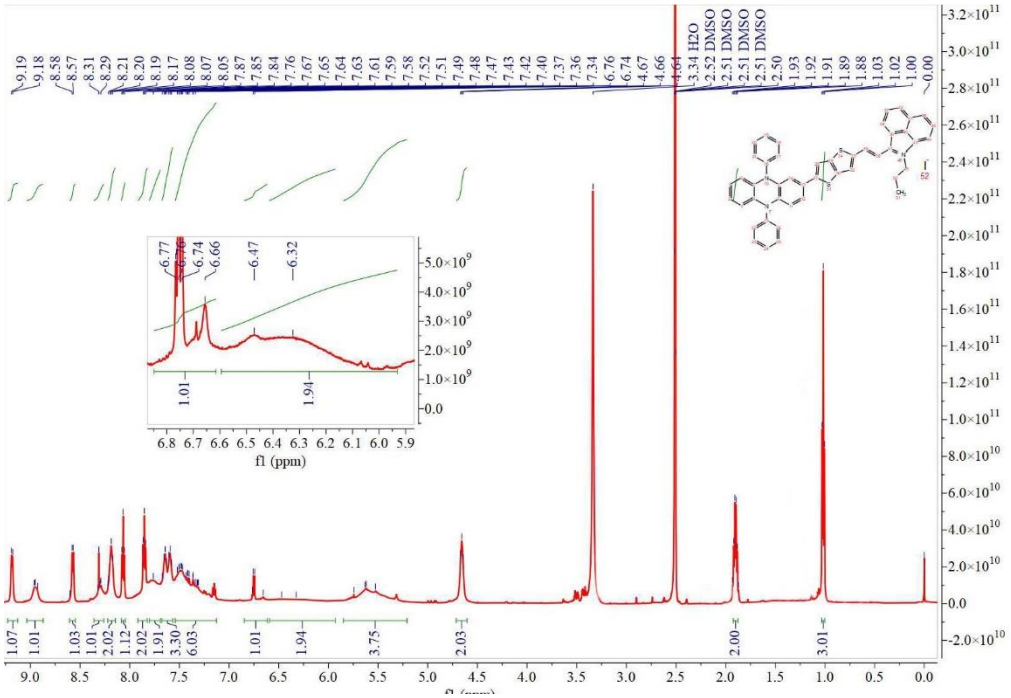

Figure S23. ^{1}H NMR spectrum of **LSC**.

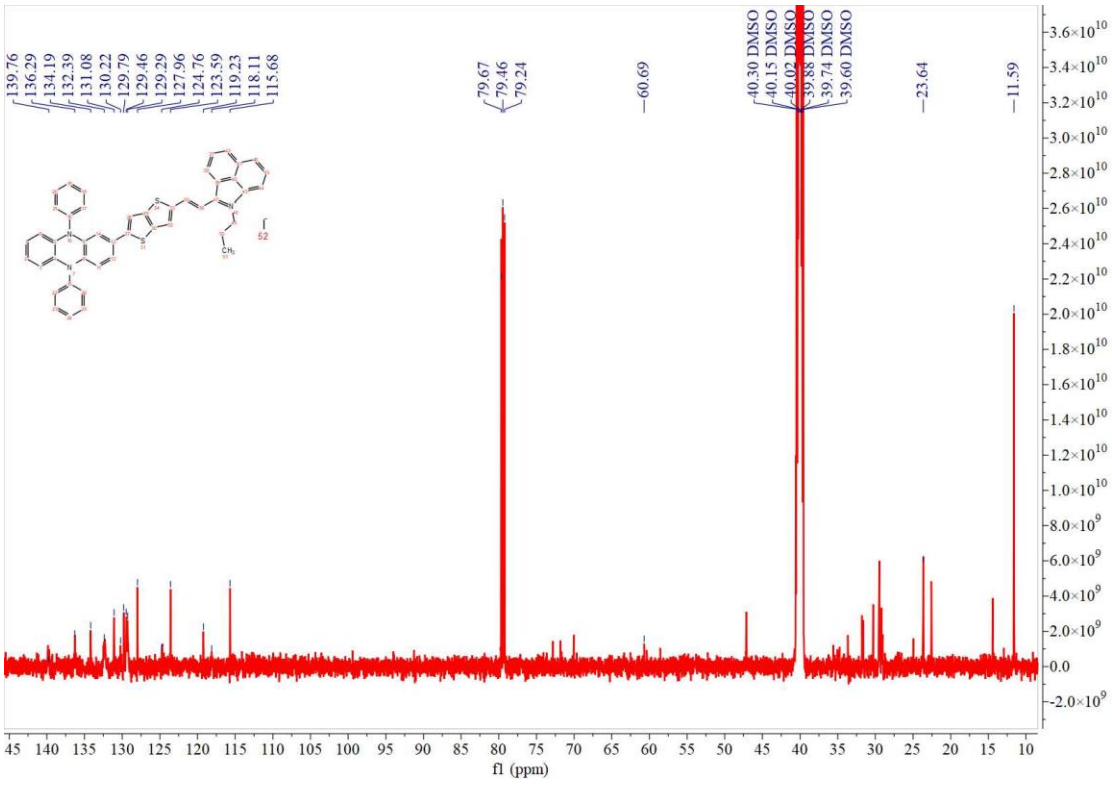

Figure S24. ^{13}C NMR spectrum of **LSC**.

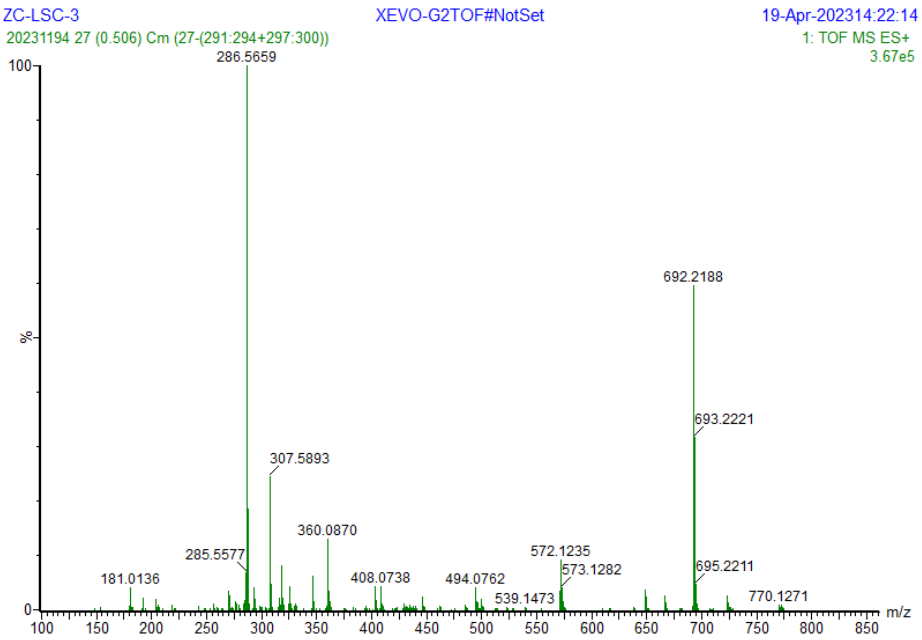

Figure S25. HRMS spectrum of **LSC**.

3. Spectra of DC, SC, and LSC in different solvents.

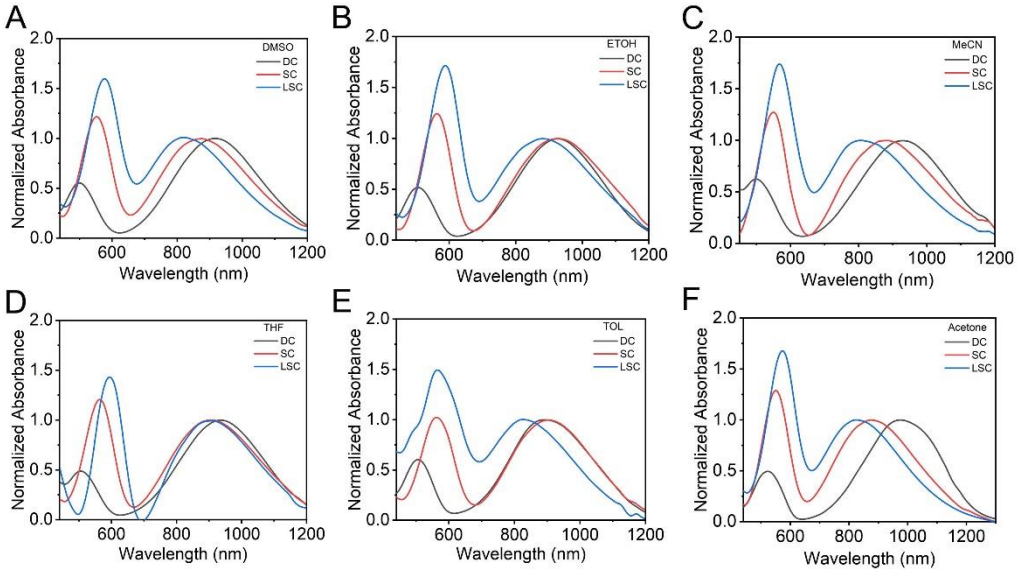

Figure S26. Absorption of **DC**, **SC**, **LSC** in different solvents; Concentration: 10 μM.

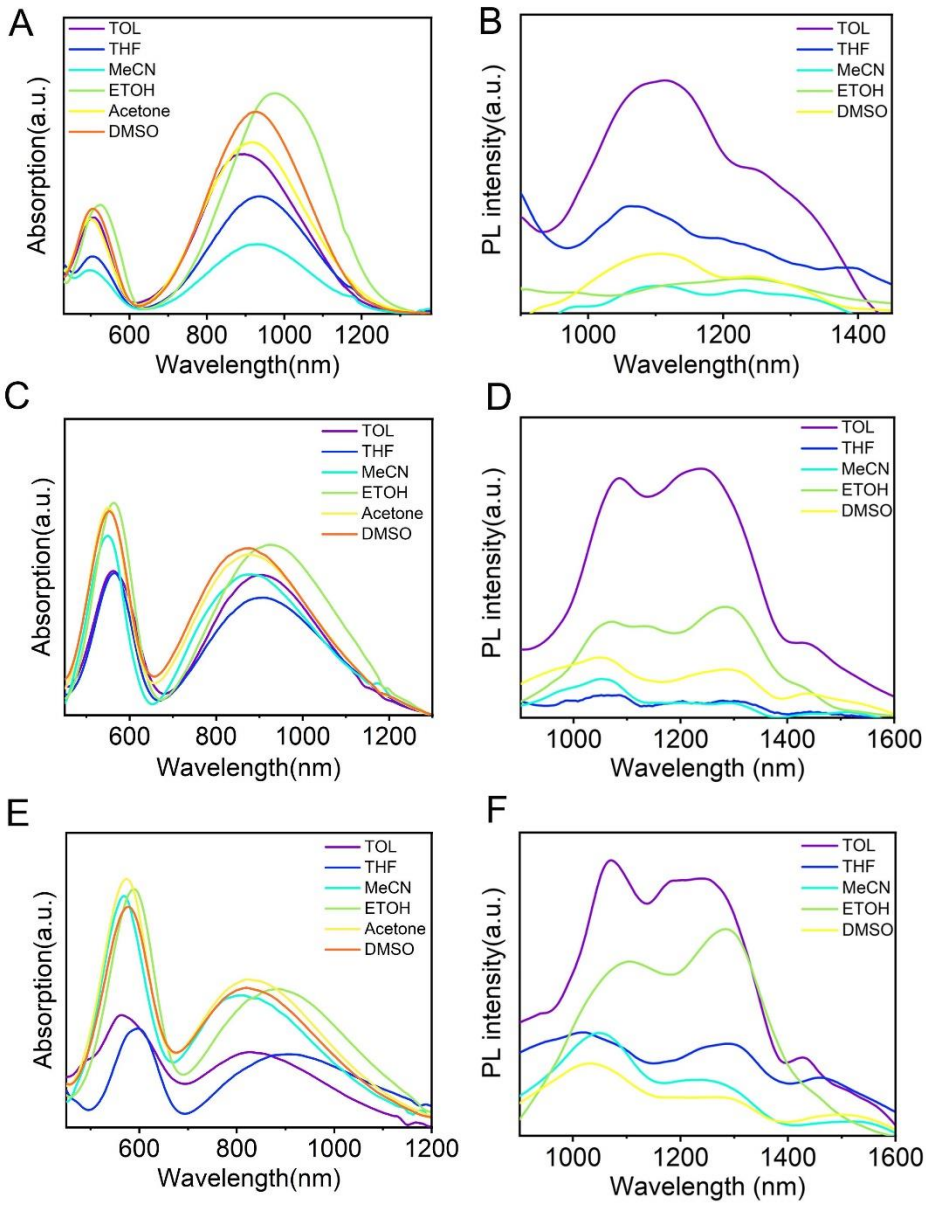

Figure S27. Absorption and emission spectra of (A, B) **DC**, (C, D) **SC**, (E, F) **LSC** in different solvents; Concentration: 10 μM.

4. Illustration of the frontier molecular orbitals.

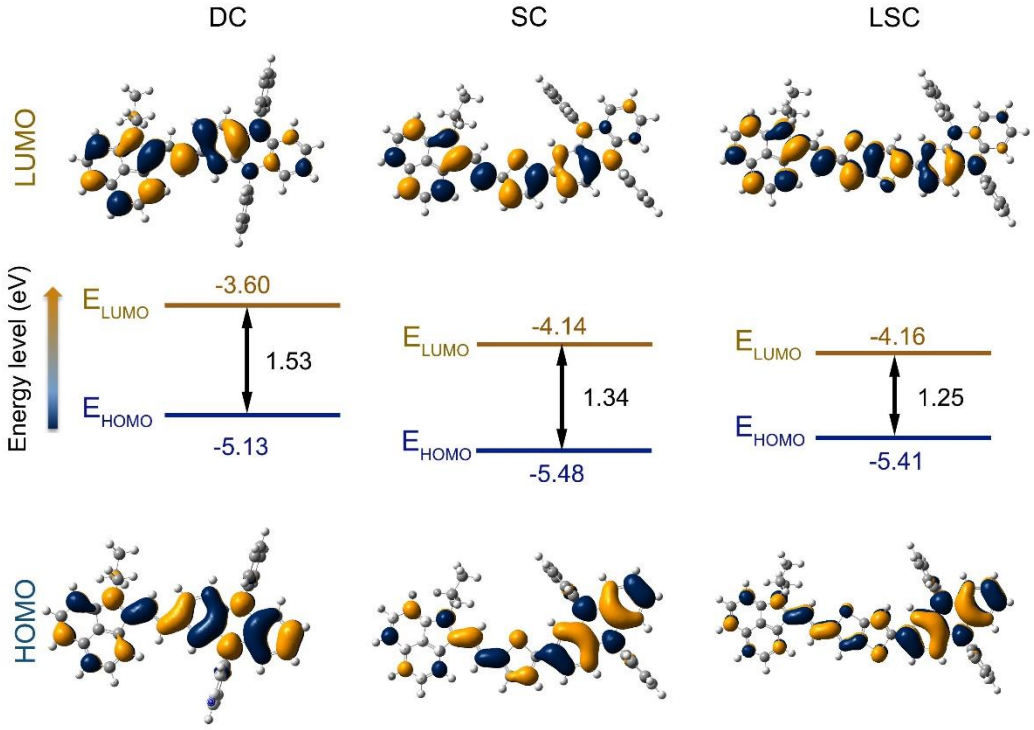

Figure S28. The electron distributions and energy levels of frontier molecular orbitals (HOMOs and LUMOs) of **DC**, **SC** and **LSC**. Illustration of the frontier molecular orbitals (LUMOs and HOMOs) determined at the B3LPY/6-31G (d, p) level of theory.

5. Spectra of concentration gradients of NPs.

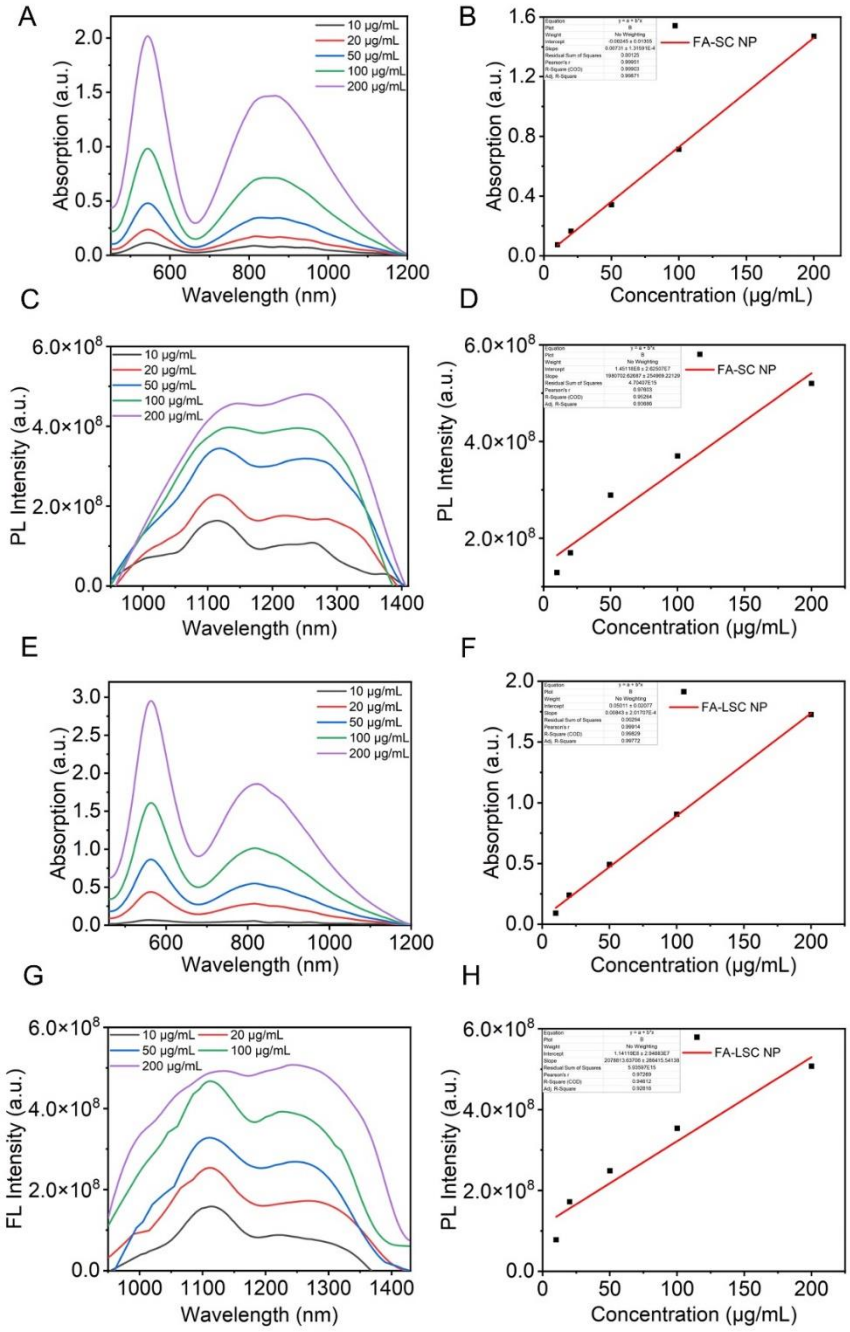

Figure S29. Absorption spectra of (A, B) **FA-SC NPs**, (E, F) **FA-LSC NPs** in PBS (left panel) and plots of absorbance values as a function of concentration (right panel). Emission spectra of (C, D) **FA-SC NPs**, (G, H) **FA-LSC NPs** in PBS (left panel) and plots of luminous intensity as a function of concentration (right panel).

6. Absorption and fluorescence spectra of DC, SC and LSC in different ratio of Toluene/ DMSO.

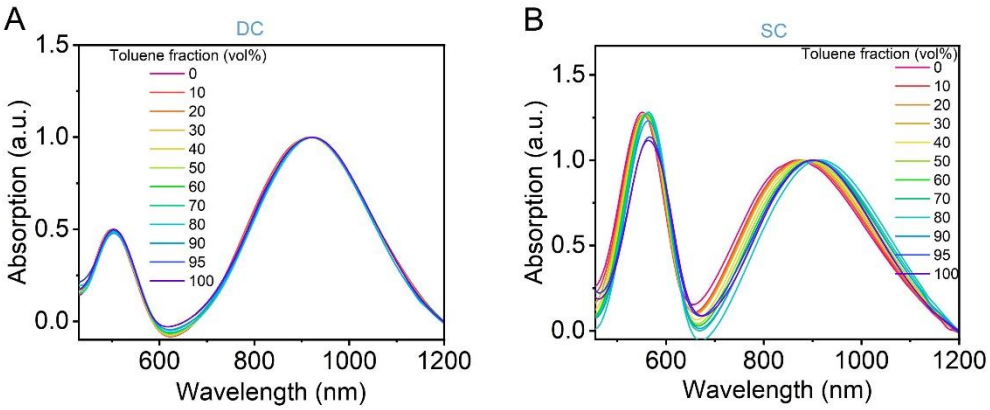

Figure S30. Absorption spectra of 10 x 10^{-6} M (A) **DC**, (B) **SC** in the mixture of Toluene/ DMSO with different fractions of Toluene (f_T).

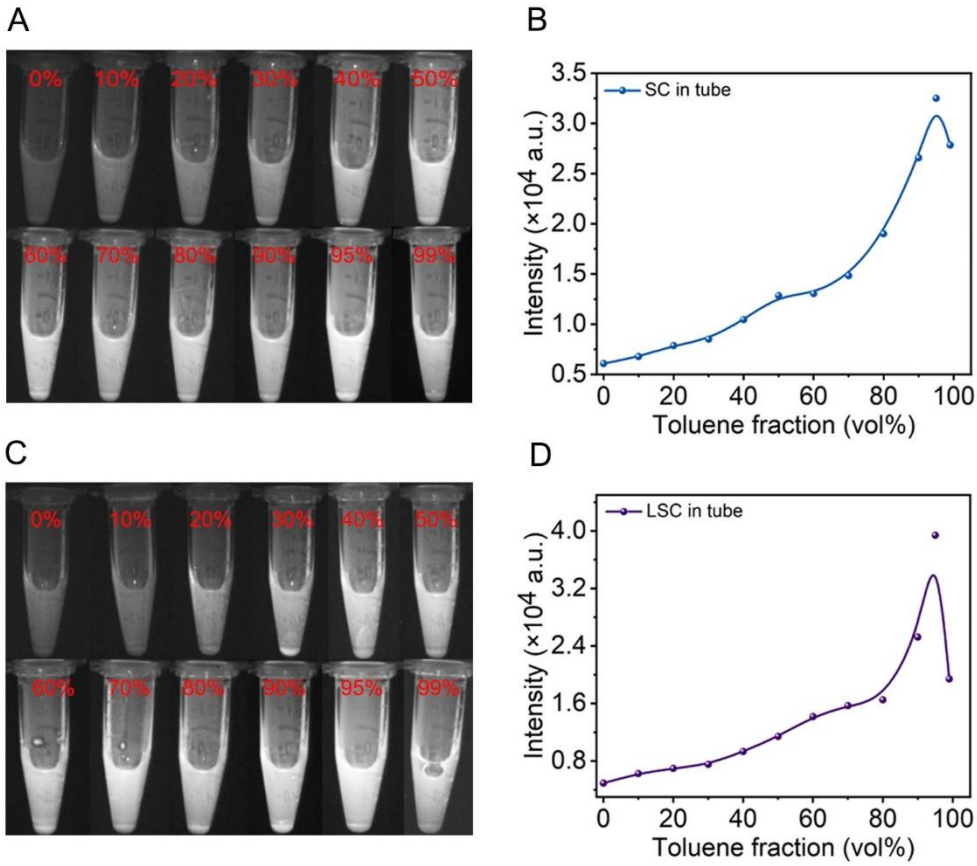

Figure S31. NIR-II fluorescence images of 10 x 10^{-6} M (A, B) **SC**, (C, D) **LSC** in the mixture of Toluene/ DMSO with different fractions of Toluene (f_T).

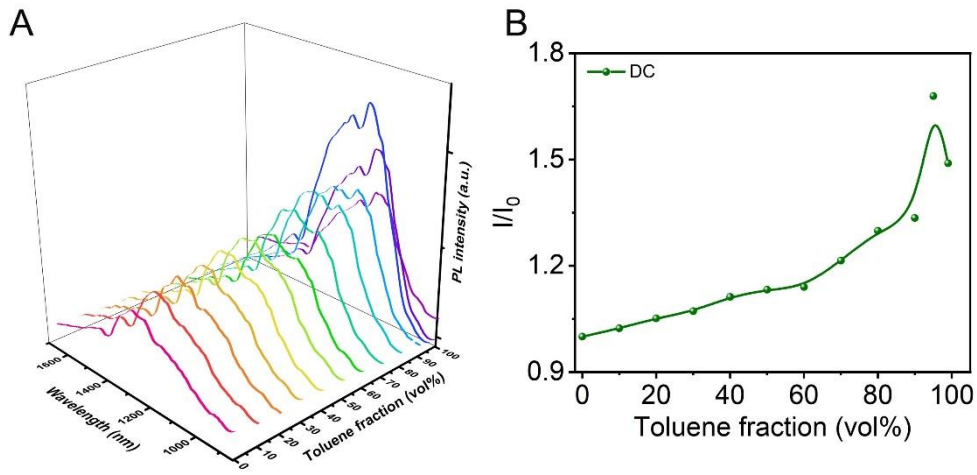

Figure S32. A) **DC** in the mixture of DMSO/Toluene with different fractions of Toluene (f_T). (λ_{ex}: 808 nm). B) Plot of the relative emission intensity (I/I_0) of A) with toluene fraction. I_0 and I are the peak values of PL intensities of **FA-DC NPs** (10×10^{-6} M) in DMSO and DMSO/Toluene mixtures, respectively.

7. The absorption and PL spectra of NPs.

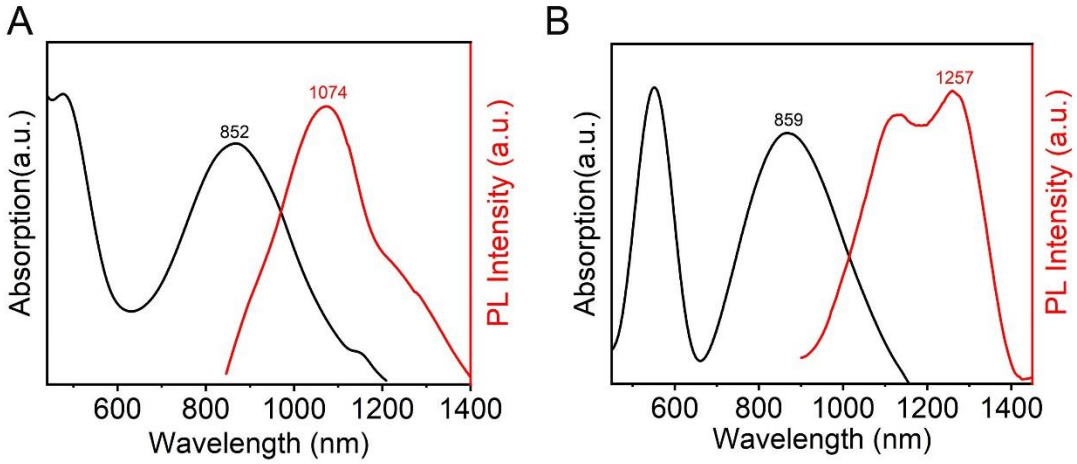

Figure S33. Absorption (black line) and emission (red line) spectra of A) **FA-DC NPs** and B) **FA-SC NPs** in aqueous solution.

8. PTT test of NPs.

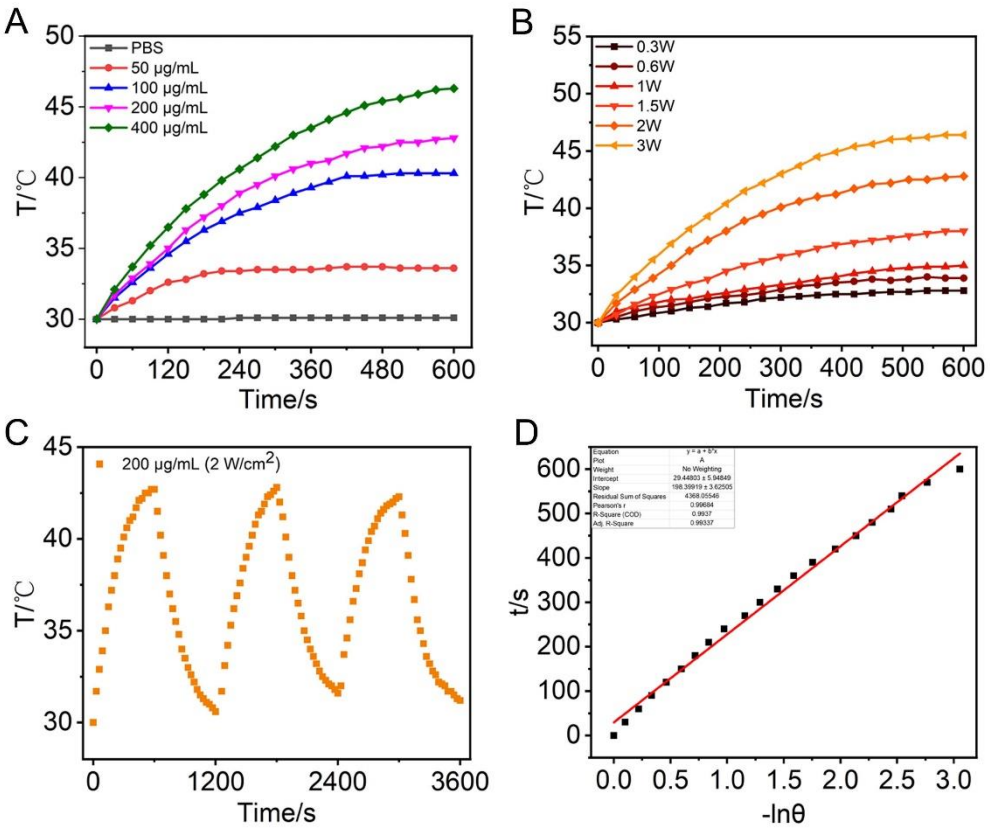

Figure S34. A) Temperature elevation for **FA-DC NPs** at different concentrations in PBS under 808 nm laser irradiation (2 W cm^{-2}); B) Laser-power-dependent temperature changes of **FA-DC NPs** (200 μg mL^{-1}) in PBS. C) The temperature changes of **FA-DC NPs** upon cyclic photothermal heating and cooling processes; the cycle was performed by laser irradiation for 10 min, then naturally cooling to room temperature. D) Relationship between t and -lnθ of **FA-DC NPs**.

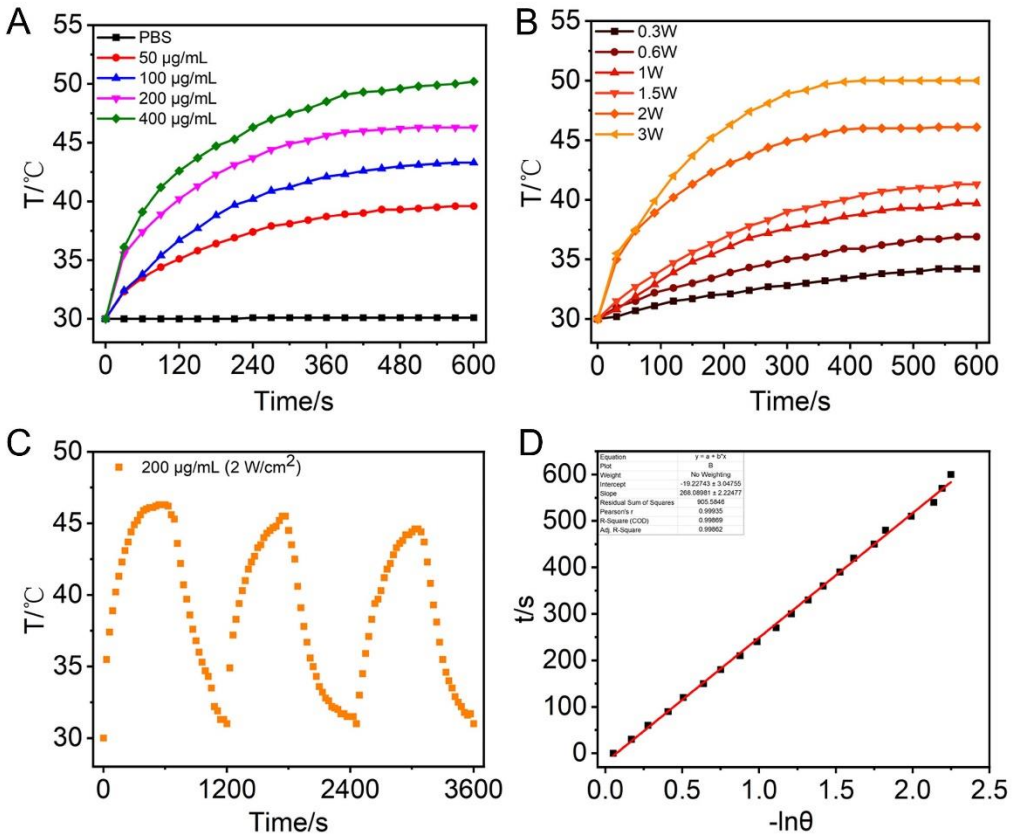

Figure S35. A) Temperature elevation for **FA-SC NPs** at different concentrations in PBS under 808 nm laser irradiation (2 W cm^{-2}); B) Laser-power-dependent temperature changes of **FA-SC NPs** (200 μg mL^{-1}) in PBS. C) The temperature changes of **FA-SC NPs** upon cyclic photothermal heating and cooling processes; the cycle was performed by laser irradiation for 10 min, then naturally cooling to room temperature. D) Relationship between t and -lnθ of **FA-SC NPs**.

The calculation method of light-to-heat conversion efficiency is as follows: First, θ is the driving temperature calculated according to Equation (2)

$$\theta = \frac{T - T_{sur}}{T_{max} - T_{sur}} \qquad (2)$$

T is the temperature corresponding to different irradiation time, T_{max} is the highest temperature of the solution after irradiation for 10 min, and T_{surr} is the initial temperature of the solution. Next, τ_s (the associated time constant of the experimental system), can be calculated according to Equation (3):

$$t = -\tau_s \ln\theta \tag{3}$$

t is the time corresponding to the cooling of the system after laser irradiation.

$$hS = \frac{mc}{\tau_s} \tag{4}$$

$$\eta = \frac{hS(T_{\max} - T_{sur}) - Q_{dis}}{I(1-10^{-A})} \tag{5}$$

Accordingly, the photothermal conversion efficiency (η) was determined according to a reported method. [1] Q_{dis} represents the heat dissipation of solvent which was measured by a power meter (VLP-2000). I is the laser power and A_λ is the absorbance at 808 nm. hS can be calculated according to Equation (4).

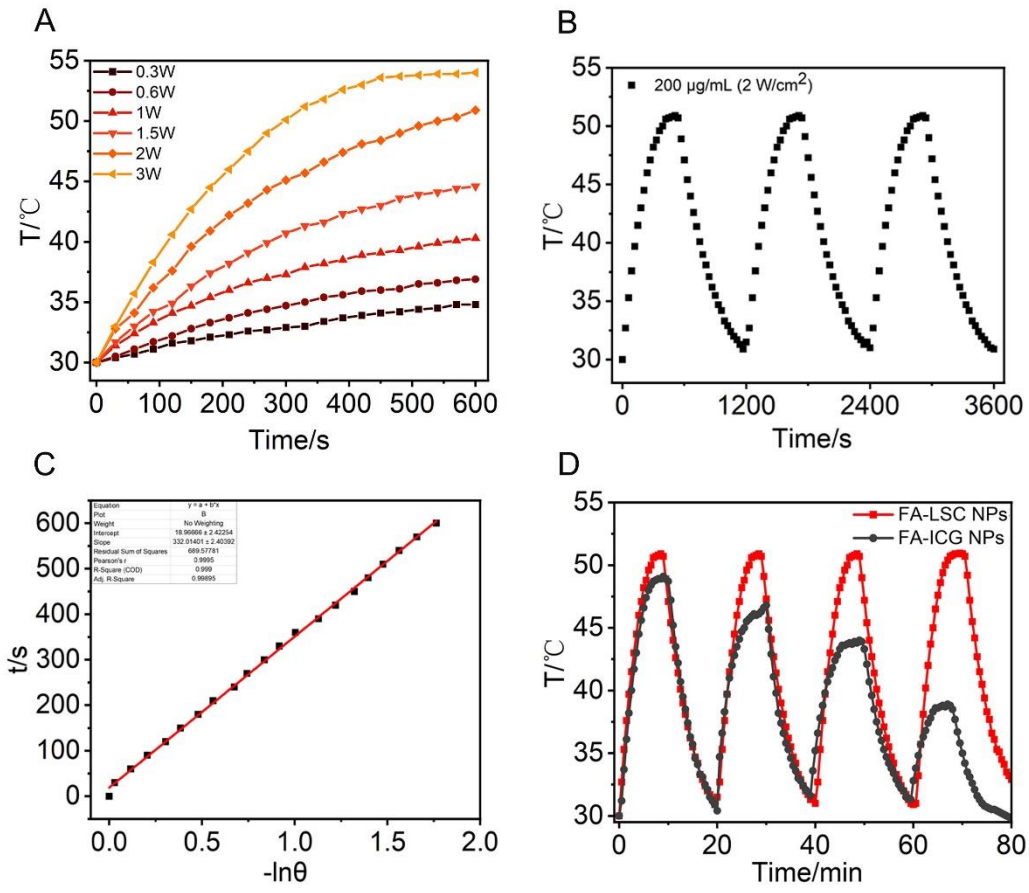

Figure S36. A) Laser-power-dependent temperature changes of **FA-LSC NPs** (200 μg mL^{-1}) in PBS. B) The temperature changes of **FA-LSC NPs** upon cyclic photothermal heating and cooling processes; the cycle was performed by laser irradiation for 10 min,

then naturally cooling to room temperature. C) Relationship between t and -lnθ of **FA-LSC NPs**. D) Photothermal stability of **FA-LSC NPs** and ICG (200 μg mL^{-1}) in aqueous solution during four on/off irradiation cycles with an 808 nm laser.

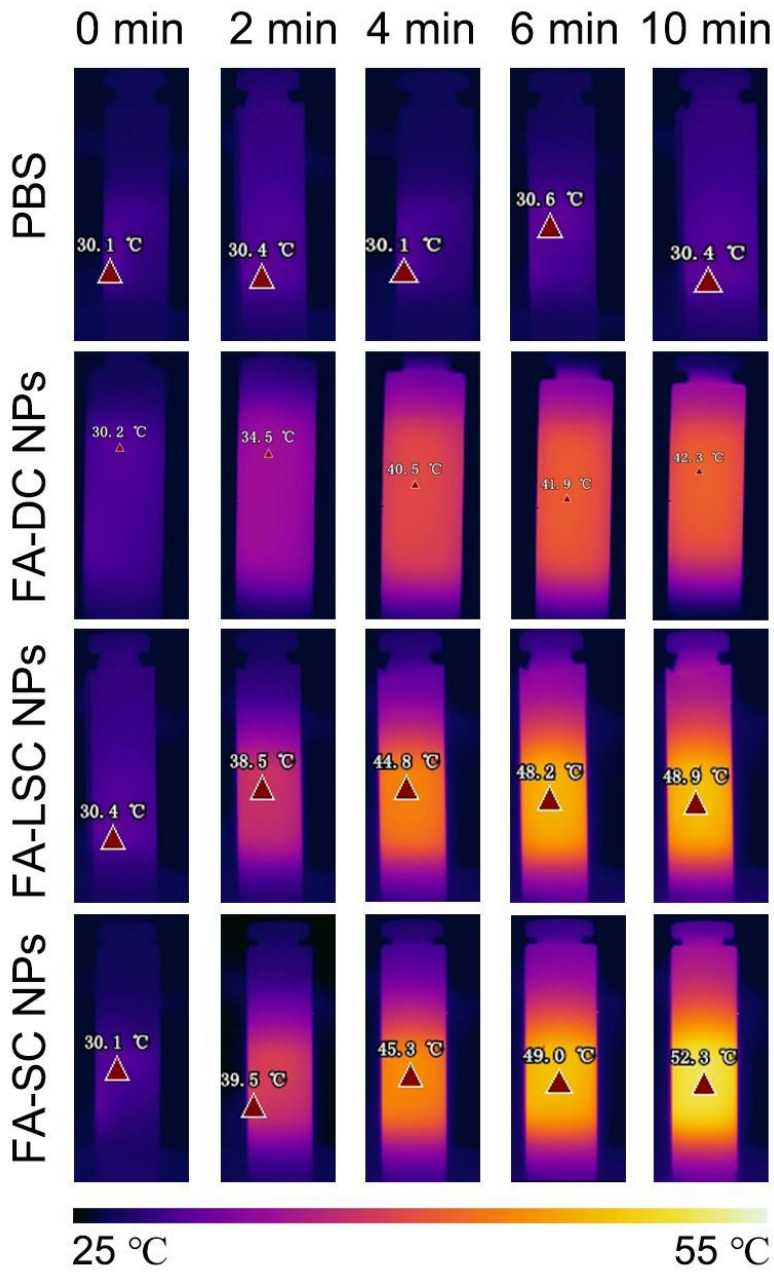

Figure S37. Corresponding thermal images of PBS, **FA-DC NPs**, **FA-SC NPs**, **FA-LSC NPs** (200 μg mL^{-1}) in aqueous solution under 808 nm laser irradiation with different time.

9. Stability test.

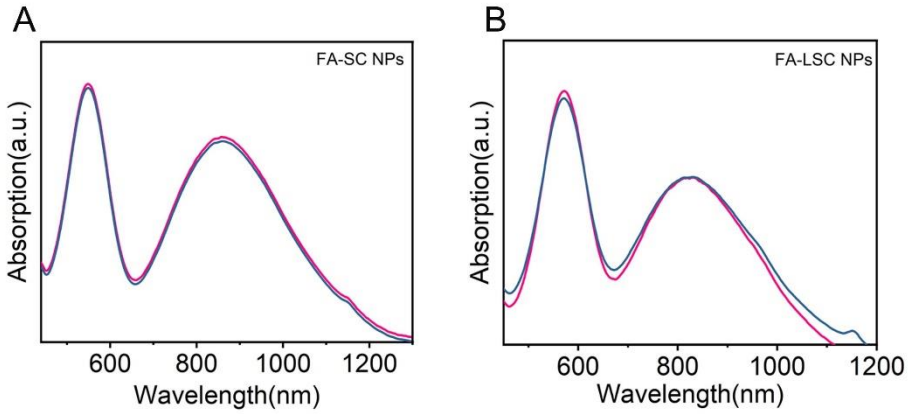

Figure S38. The absorption changes of **FA-SC NPs** A) and **FA-LSC NPs** B) under continuous irradiation with an 808 nm laser (2 W cm^{-2}).

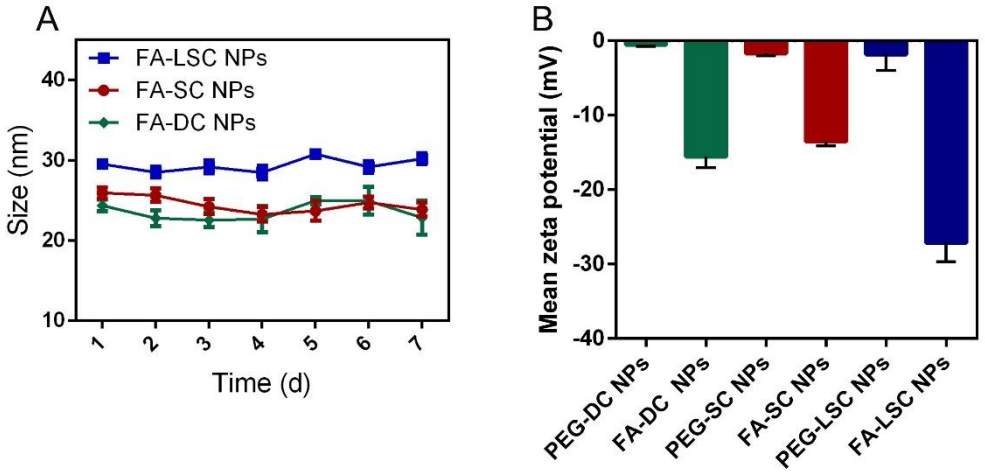

Figure S39. A) Stability analysis for size variation of **FA-DC NPs**, **FA-SC NPs** and **FA-LSC NPs** with a concentration of 200 μg mL^{-1} at room temperature in PBS measured by DLS. B) Zeta potential of NPs determined by DLS with a concentration of 200 μg mL^{-1} in aqueous medium. (means ± SD, n = 3)

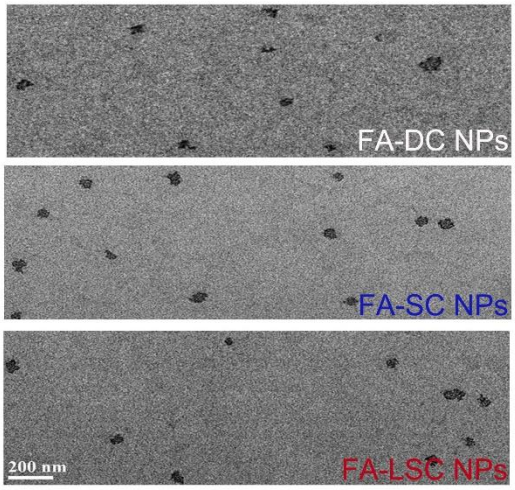

Figure S40. TEM images of corresponding NPs.

10. Relative fluorescence quantum yield.

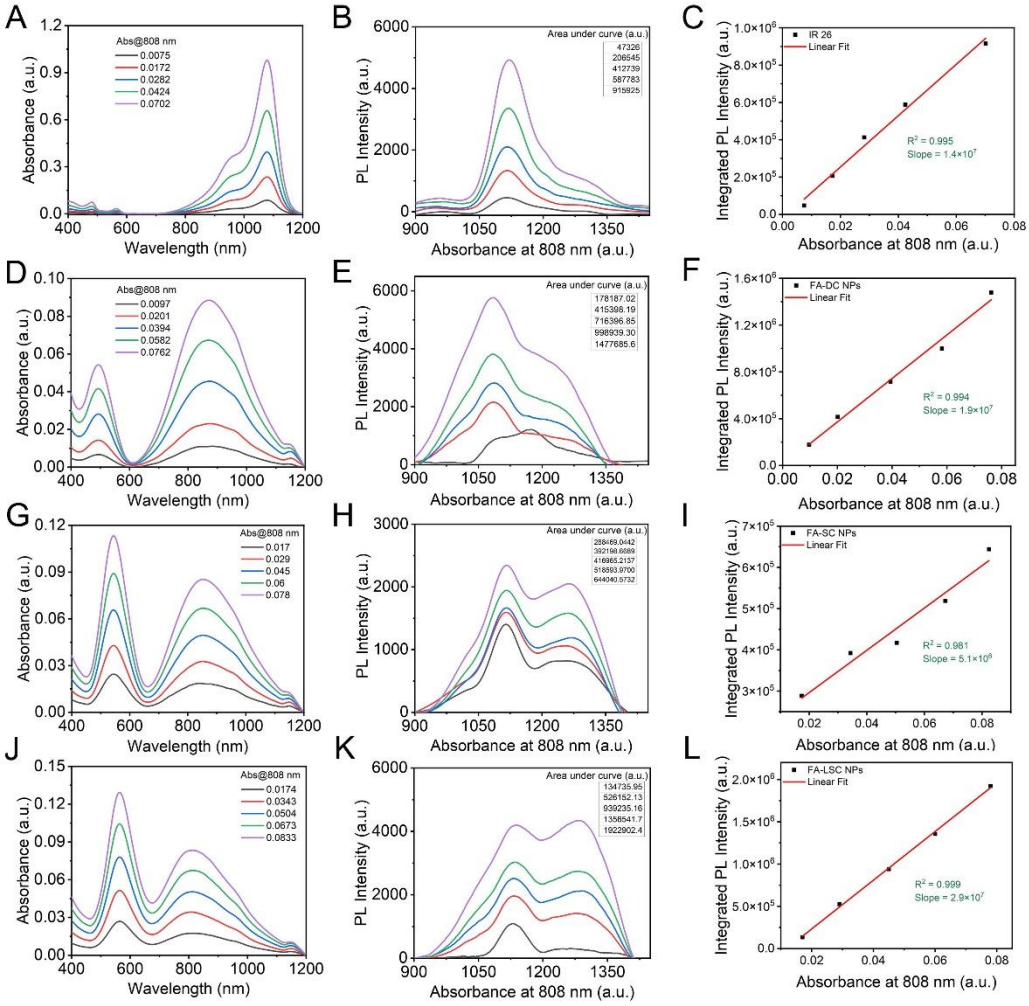

Figure S41. Fluorescence QYs of **FA-DC NPs**, **FA-SC NPs** and **FA-LSC NPs** in

aqueous solutions. (A) UV-Vis-NIR absorption spectra of IR-26 in 1,2-dichloroethane (DCE) with absorbance values at 808 nm. The exact absorbance of each solution was listed in the inset table. (B) NIR-II emission spectra of five solutions in (A). Their fluorescence emission spectra in the 900 - 1450 nm range was taken under 808 nm laser excitation. Area under curve in the emission spectrum for each solution was then calculated and listed in the inset table. (C) For all DCE solutions of IR-26, their absorbance values were then plotted versus area under curve in the emission spectrum, and fitted into a linear function, where slope of the fitted line was read as shown. The same absorption and emission measurements, linear fitting curves were performed for **FA-DC NPs** (D-F), **FA-SC NPs** (G - I) and **FA-LSC NPs** (J – L) in aqueous solutions.

Dye	Type	Solvent	ε ($M^{-1}cm^{-1}$)	λ_{abs} (nm)	λ_{em} (nm)	Φ (%)	$\varepsilon\Phi$ ($M^{-1}cm^{-1}$)	Reference
IR 26	D-A-D[a]	PBS	3750	1080	1095	0.01	0.375	[5]
CF1065	D-A-D	PBS	13100	820	1090	<0.01	-	[6]
FM1210	D-A-D	PBS	10900	930	1250	<0.01	-	[6]
FT-TQT	D-A-D	PBS	8940	770	1034	0.025	2.235	[7]
BTC1070	D-A-D	PBS	45000	1015	1065	0.01	0.375	[5]
DPBTA-DPTQ	D-π-A-π-D	PBS	10400	806	1120	0.16	16.64	[8]
DPA-3	A-D-D´[b]	DMSO	53000	810	1050	0.07	37.1	[9]
DPA-4	A-D-D´	DMSO	21800	845	1050	0.05	10.93	[9]
IR-FTAP	S-D-A-D-S[c]	Water	5000	733	1048	0.53	26.5	[10]
CH4T	D-A-D	PBS	10000	738	1055	1.08	108	[11]
IR-BEMC6P	S-D-A-D-S	PBS	2420	737	1028	1.8	43.6	[12]
dBTIC-D NPs	A-D-A	PBS	140000	732	1048	2.0	2900	[13]
IDT-TPE NPs	A-D-A	PBS	89000	687	834	1.7[d]	1513	[14]
FA-DC NPs	D-π-A	PBS	52000	870	1074	0.57	296.4	
FA-SC NPs	D-π-A	PBS	89000	859	1257	0.16	142.4	This work
FA-LSC NPs	D-π-A	PBS	121000	825	1278	0.88[e]	1064.8	

[a)] Donor-Acceptor-Donor (D-A-D) [b)] Acceptor-Donor-Donor´ (A-D-D´) [c)] Shielding units (S) to construct S-D-A-D-S type. [d)] The PLQY is absolute QY. [e)] The PLQY reference is the IR26 of 0.5%.

Table S1. Photophysical properties of previously reported dyes in aqueous.

11. FA-ICG NPs targeting ability test.

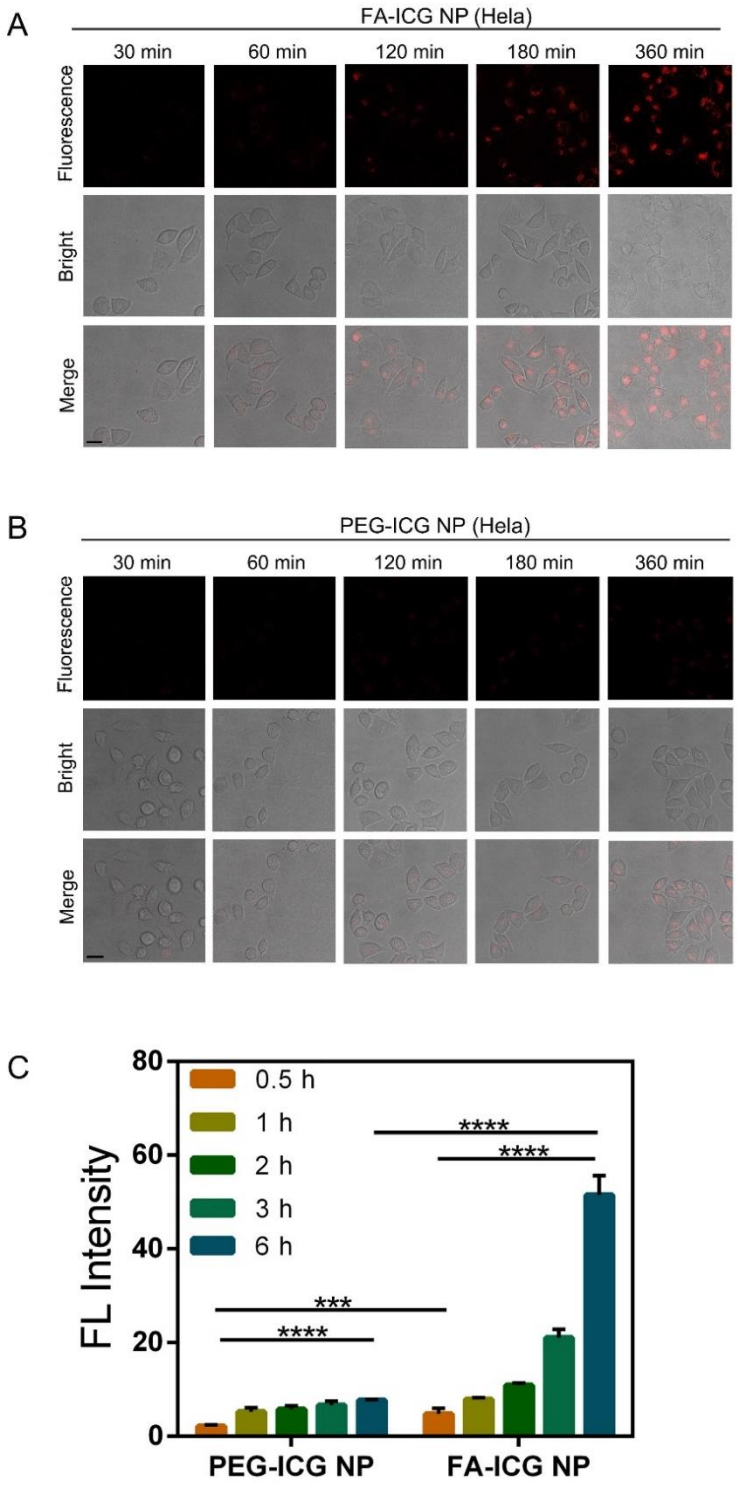

Figure S42. Confocal fluorescence imaging of Hela cells uptake of A) FA-ICG NPs, B) PEG-ICG NPs. Scale bar = 20 μm. C) Quantitative analysis of A), B) results of Hela cells uptake of FA-ICG NPs, PEG-ICG NPs. (means ± SD, n = 5, C_{ICG} = 200 μg mL^{-1}). ***p < 0.001, ****p < 0.0001.

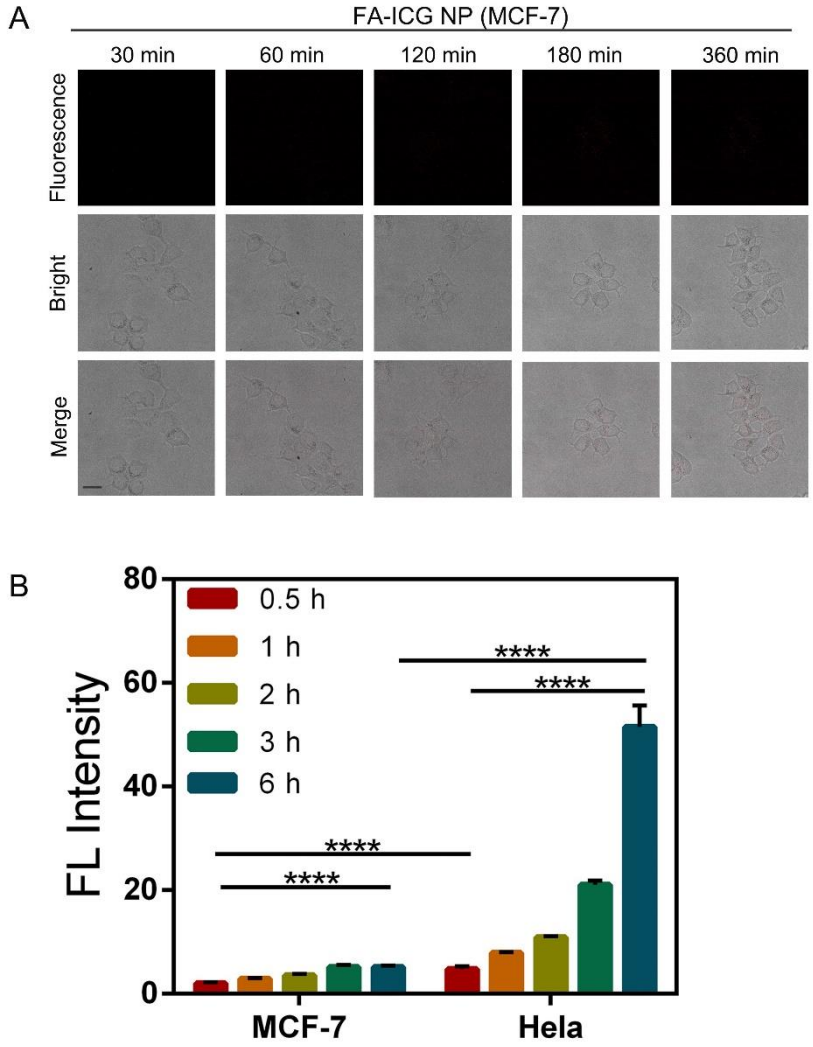

Figure S43. Confocal fluorescence imaging of MCF-7 cells uptake of A) FA-ICG NPs. Scale bar = 20 μm. B) Quantitative analysis of A) results of MCF-7 cells uptake of FA-ICG NPs. (means ± SD, n = 5, C_{ICG} = 200 μg mL^{-1}). ***p < 0.001, ****p < 0.0001.

12. Live/dead fluorescence images.

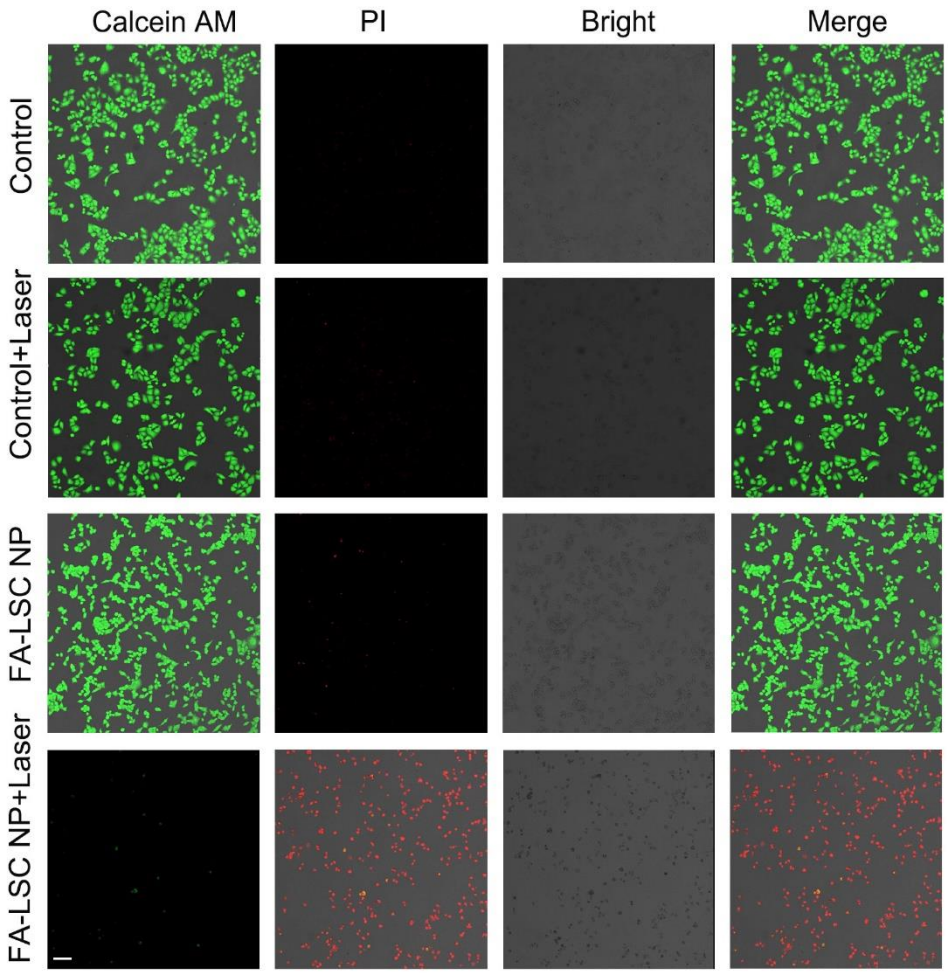

Figure S44. Live/dead images of Hela cells after various treatments. The green fluorescence from Calcein-AM and red fluorescence from PI represent live cell and dead cells, respectively. Scale bars: 50 μm.

13. In vivo imaging and therapeutic efficacy of FA-LSC NPs in photothermal therapy.

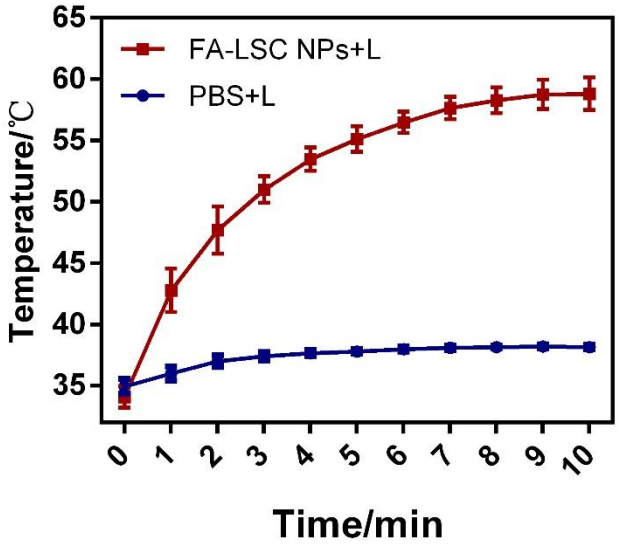

Figure S45. In vivo photothermal images of Hela tumor-bearing mice at different time points during 808 nm laser irradiation (2 W cm^{-2}) 12 h after intravenous injection of **FA-LSC NPs** and saline. The corresponding statistic temperature changes at the tumor sites during the continuous laser irradiation. (means ± SD, n = 3).

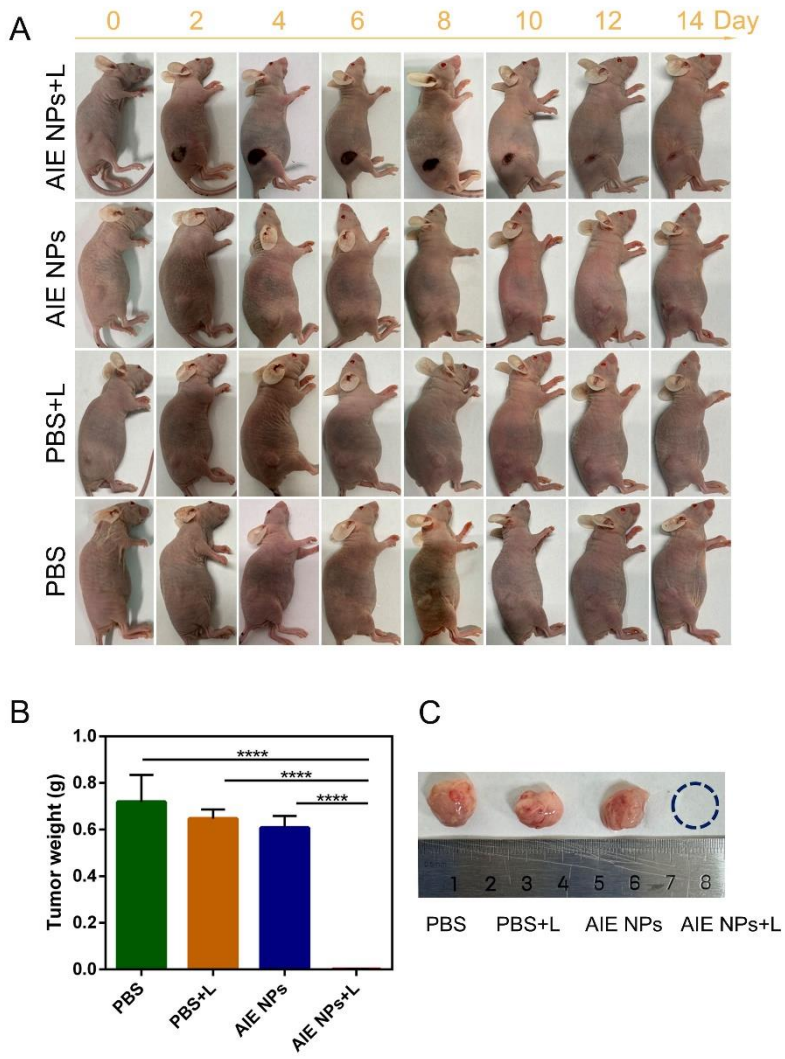

Figure S46. A) Photos of treated mice 808 nm laser irradiation with a power density of 2 W cm^{-2} was performed at 12 h post-administration of **FA-LSC NPs** (200 μg mL^{-1}), each group was recorded for 14 days. B) Tumor weight in different groups was obtained on day 14 and C) the representative photographs of tumor tissues on day 14. Data are represented as mean ± SD (n = 4). ****$p < 0.0001$.

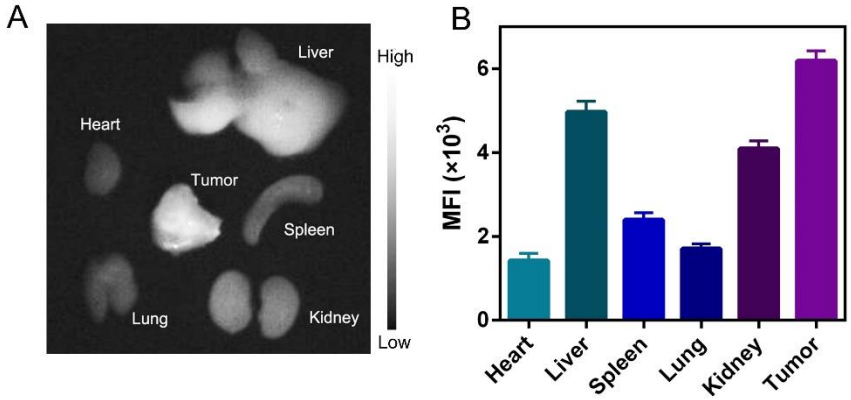

Figure S47. A) Ex vivo NIR-II fluorescence images and B) the corresponding mean fluorescence intensity (MFI) of tumor and major organs after intravenous injection with **FA-LSC NPs** for 12 h. (means ± SD, n = 3).

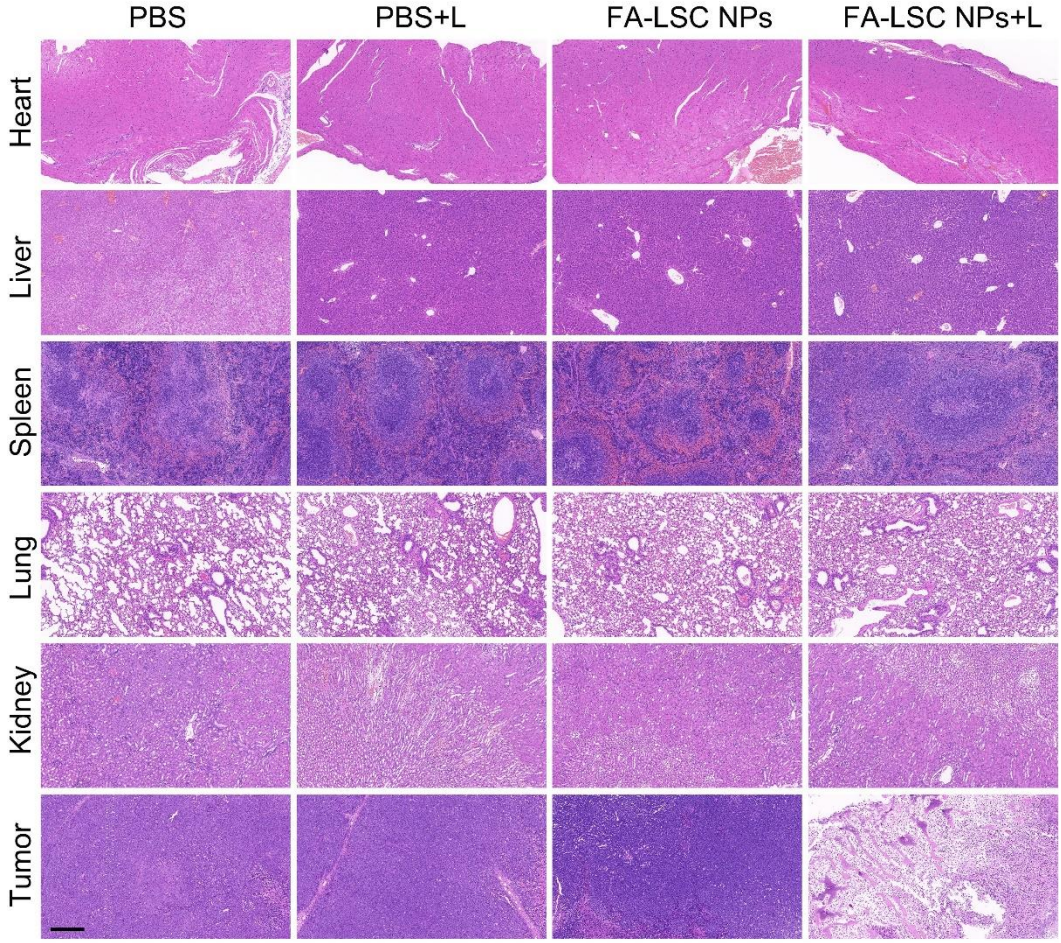

Figure S48. H&E staining for tumors of mice after various treatments and major organs of mice without treatment and treated with **FA-LSC NPs** and 808 nm light irradiation. Scale bar = 100 μm.

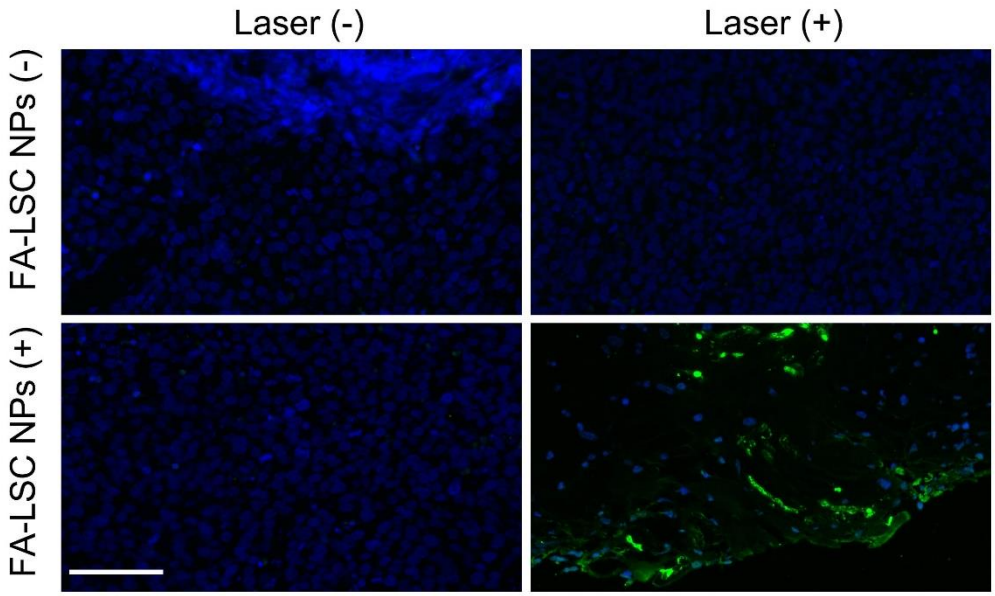

Figure S49. Tunel staining for tumors of mice after various treatments without treatment and treated with **FA-LSC NPs** and 808 nm light irradiation. Scale bar = 20 μm.

14. References

[1] Frisch, M. J. et al. Gaussian 16, Revision A.03, 2016.

[2] T. Lu, F. Chen, *J. Comput. Chem.* 2012, **33**, 580.

[3] J. Sun, N. Cheng, K. Yin, R. Wang, T. Zhu, J. Gao, X. Dong, C. Dong, X. Gu and C. Zhao, Activatable photothermal agents with target-initiated large spectral separation for highly effective reduction of side effects, *Chem. Sci.* 2022, **13**, 9525-9530.

[4] Q. Wan, Y. Li, K. Ding, Y. Xie, J. Fan, J. Tong, Z. Zeng, Y. Li, C. Zhao, Z. Wang and B. Z. Tang, Aggregation Effect on Multiperformance Improvement in Aryl-Armed Phenazine-Based Emitters, *J. Am. Chem. Soc.* 2023, **145,** 1607-1616.

[5] S. Wang, Y. Fan, D. Li, C. Sun, Z. Lei, L. Lu, T. Wang and F. Zhang, Anti-quenching NIR-II molecular fluorophores for in vivo high-contrast imaging and pH sensing, *Nat. Commun*. 2019, **10**, 1058.

[6] Y. Fang, J. Shang, D. Liu, W. Shi, X. Li and H. Ma, Design, Synthesis, and Application of a Small Molecular NIR-II Fluorophore with Maximal Emission beyond 1200 nm, *J. Am. Chem. Soc.* 2020, **142**, 15271-15275.

[7] A. Ji, H. Lou, C. Qu, W. Lu, Y. Hao, J. Li, Y. Wu, T. Chang, H. Chen and Z. Cheng, Acceptor engineering for NIR-II dyes with high photochemical and biomedical performance, *Nat. Commun*. 2022, **13,** 3815.

[8] D. Yan, W. Xie, J. Zhang, L. Wang, D. Wang and B. Z. Tang, Donor/pi-Bridge Manipulation for Constructing a Stable NIR-II Aggregation-Induced Emission Luminogen with Balanced Phototheranostic Performance*, *Angew. Chem*. 2021, **60**, 26769-26776.

[9] X. Zhao, J. Cheng, L. Zhang, B. Yun, K. Yan, B. Wu, X. Liu, F. Zhang and Z. Lei, Near-infrared II emissive diphenylaminoacridine based on the planarized intramolecular charge transfer mechanism, *Cell Reports Physical Science,* 2023, **4**.

[10] Q. Yang, Z. Hu, S. Zhu, R. Ma, H. Ma, Z. Ma, H. Wan, T. Zhu, Z. Jiang, W. Liu, L. Jiao, H. Sun, Y. Liang and H. Dai, Donor Engineering for NIR-II Molecular Fluorophores with Enhanced Fluorescent Performance, *J. Am. Chem. Soc.* 2018, **140**, 1715-1724.

[11] A. L. Antaris, H. Chen, S. Diao, Z. Ma, Z. Zhang, S. Zhu, J. Wang, A. X. Lozano, Q. Fan, L. Chew, M. Zhu, K. Cheng, X. Hong, H. Dai and Z. Cheng, A high quantum yield molecule-protein complex fluorophore for near-infrared II imaging, *Nat. Commun*. 2017, **8**, 15269.

[12] R. Tian, H. Ma, Q. Yang, H. Wan, S. Zhu, S. Chandra, H. Sun, D. O. Kiesewetter,

G. Niu, Y. Liang and X. Chen, Rational design of a super-contrast NIR-II fluorophore affords high-performance NIR-II molecular imaging guided microsurgery, *Chem. Sci.* 2019, **10,** 326-332.

[13] H. Li, Q. Li, Y. Gu, M. Wang, P. Tan, H. Wang, L. Han, Y. Zhu, F. He and L. Tian, Dimerization extends π-conjugation of electron donor-acceptor structures leading to phototheranostic properties beyond the sum of two monomers, *Aggregate,* 2024, DOI: 10.1002/agt2.528.

[14] D. Li, Y. Li, Q. Wu, P. Xiao, L. Wang, D. Wang and B. Z. Tang, Add the Finishing Touch: Molecular Engineering of Conjugated Small Molecule for High-Performance AIE Luminogen in Multimodal Phototheranostics, *Small,* 2021, **17**.